Temperature and pressure dependence of the transverse-optic modes of ionic crystals and their associated anharmonic self-energies*

R. P. Lowndes† and A. Rastogi
Physics Department, Northeastern University, Boston, Massachusetts 02115
(Received 15 March 1976)

The temperature dependence (2–300 K) and hydrostatic pressure dependence (0–7 kbar) of the $q \approx 0$ transverse-optic mode frequency ω_t and its associated damping $2\Gamma(0, t, \omega_t)$ are reported for the alkali, silver, and thallium halides. These results are analyzed to yield the temperature dependence of the thermal strain $\Delta^E(0, t)$ and far-infrared anharmonic self-energies $\Delta_T^A(0, t, \omega_t)$ associated with the mode at ω_t. In addition, calculations of $\Delta^E(0, t)$, $\Delta_T^A(0, t, \Omega)$ at $\Omega = 0$ and $\Omega = \omega_t$, and $\Gamma(0, t, \omega_t)$ are presented for the alkali halides crystallizing in the NaCl structure using current many-body thermodynamic Green's-function anharmonic theories, and these are compared with the experimental results.

I. INTRODUCTION

The interatomic forces in a crystal are usually strongly dependent on the interatomic spacing and consequently the lattice potential energy for a crystal can generally be written as a power series in the displacements of the atoms from their equilibrium positions. If such an expansion is terminated at the quadratic terms, then this constitutes the so-called harmonic approximation. In the harmonic approximation the lattice vibrations are true normal modes such that if energy is channeled uniquely into any one lattice mode, then it will remain undissipated in that mode. The harmonic approximation would therefore predict, for instance, that the spectral profiles of lattice vibrations would be a set of undamped, temperature-independent resonances. These and other such predictions are, of course, in marked discord with experimental evidence. As a result, the anharmonic terms in a lattice potential must be considered if a full understanding of many of the physical properties of solids is to be achieved.

The inclusion of the anharmonic terms in a lattice potential has two main consequences. First, the phenomenon of thermal expansion is now allowed. Second, the anharmonicity allows interactions between the normal modes. The net effect of these interactions is to open up channels for the decay of phonons which lead to changes in the phonon energies together with the appearance of finite lifetimes for the phonons.[1,2] The temperature dependence of each phonon energy in the Brillouin zone therefore arises in two separate ways from lattice anharmonicity. First, the thermal expansion arising from the anharmonicity creates a temperature-dependent shift of each phonon energy from the harmonic normal mode value. Second, the anharmonic interactions between phonons cause a further temperature-dependent shift for the phonon energies which can be distinguished from the effects of thermal strain because the former effect gives rise to a temperature dependence of the phonon self-energies that takes place even when the crystal is held under isochoric conditions.

The determination of these anharmonic self-energies has proved to be no easy matter on either theoretical or experimental grounds. Theoretical descriptions of anharmonic self-energies involve many-body thermodynamic Green's-function approaches, and quantitative theoretical estimates require complex calculations which need significant computational times. As a result, reports of such calculations have been somewhat limited[2-6] and these have been confined to a few simple ionic compounds. Because of their complicated form and the need to separate out the effects of the thermal strain, experimental measurements do not lead straightforwardly to determinations of the anharmonic self-energies. Lowndes and Martin[7] have suggested an experimental approach using high-pressure and variable-temperature measurements to overcome these problems and have utilized it via dielectric-constant measurements to make first estimates of the low-frequency anharmonic self-energies of the $q \approx 0$ transverse-optic phonons in simple ionic solids. But the anharmonic self-energies are frequency dependent and their measurement at other frequencies is needed in order to more fully test current anharmonic theories. Although the procedure outlined by Lowndes and Martin[7] lends itself to such a measurement, the technical difficulties increase significantly as the frequency is raised at which the anharmonic self-energy measurements are to be made. One of the prime technical difficulties is associated with an accurate determination of the thermal-strain contribution. Although the thermal-strain contribution can be determined from low-frequency dielectric-constant measurements, it is more directly determined from high-pressure

spectroscopic studies on specific phonons.[8,9] Unfortunately, the technical problems associated with maintaining reasonable signal-to-noise levels in passing radiation from the comparatively weak far-infrared or neutron sources through a high-pressure cell have proved difficult to overcome.

In this paper we describe a high-pressure far-infrared experiment which has overcome these difficulties and allowed us to measure the thermal strain and far-infrared anharmonic self-energies associated with the $q \approx 0$ transverse-optic phonons for a wide range of alkali and heavy-metal halides. In addition, we report on numerical estimates of the anharmonic self-energies for those alkali halides crystallizing in the NaCl structure and use these in a comparison with the experimental results as a first test of current theories of anharmonicity.

II. THEORETICAL CALCULATIONS

A. Introduction

In describing the physical properties of a real anharmonic crystal it is usual to resort to the use of perturbation theory. While ordinary perturbation theory has been used to describe anharmonic interactions,[10-12] more recent discussions have appealed to the techniques of quantum field theory in which the system is described in terms of the Green's functions or propagators for the system. The use of temperature-dependent time-ordered Green's functions to describe anharmonic interactions between normal modes of vibration has been described by Maradudin and Fein[1] and Cowley.[2] These authors have shown that the dielectric and scattering properties (which are of interest here) of an anharmonic crystal are dependent on the Fourier transforms of certain time correlation functions, the simplest of which is the one-phonon Green's function defined by

$$G(\vec{q}, jj', t) = \langle TA(\vec{q}, j, t)A^*(\vec{q}, j', 0)\rangle , \tag{1}$$

where the phonon operator $A(\vec{q}, j)$ is defined in terms of the sum of a creation and destruction operator, T is the Dyson time-ordering parameter, and the triangular parentheses represent thermal averaging. These Green's functions are periodic in the complex time direction and can be expanded in a Fourier series in that direction. The coefficients of this series are

$$G(\vec{q}, jj', \Omega) = \frac{i}{\beta\hbar} \int_0^{-i\beta\hbar} G(\vec{q}, jj', t)e^{i\Omega t}\, dt , \tag{2}$$

where $\beta = 1/kT$, k being Boltzmann's constant, and $\Omega = 2\pi x i/\beta\hbar$, x being an integer. The physical properties of the crystal can be obtained from these coefficients, analytically continued over the whole of the complex ω plane. The coefficients are obtained from the use of diagrammatic perturbation theory and the Dyson equation for the Green's functions obtained from these diagrams is the matrix equation

$$\sum_{j'} (\{[\omega^h(\vec{q}, j)]^2 - \Omega^2\}\delta_{jj'} + 2\omega^h(\vec{q}, j)D(\vec{q}, jj', \Omega)) \times G(\vec{q}, j'j'', \Omega) = \frac{\delta_{jj''} 2\omega^h(\vec{q}, j)}{\beta\hbar} , \tag{3}$$

where $D(\vec{q}, jj', \Omega)$ is the anharmonic self-energy of of the phonons. In the harmonic approximation the self-energy $D(\vec{q}, jj', \Omega)$ is zero and the left-hand side of Eq. (3) then plays the role of the dynamical matrix within the harmonic approximation. In the anharmonic crystal the self-energy is not zero and the matrix on the left-hand side of Eq. (3) couples phonons from the dispersion branches j, j', and j'' with the same wave vector. This coupling will occur whenever the modes transform according to the same irreducible representation of the space group of the crystals. The matrix $D(\vec{q}, jj', \Omega)$ has Hermitian and anti-Hermitian parts, the Hermitian parts giving rise to a shift in the normal mode frequencies, and the anti-Hermitian parts giving rise to a now finite lifetime for the phonon state. Formally the anharmonic contribution to the Hermitian part of the self-energies of the normal modes can be included by renormalizing the frequencies and eigenvectors of the normal modes. If the off-diagonal Hermitian terms in the matrix equation are neglected, then the Green's function for the anharmonic crystal becomes similar to that of the harmonic crystal if $[\omega^h(\vec{q}, j)]^2$ is replaced by $[\omega(\vec{q}, j)]^2$ such that

$$[\omega(\vec{q}, j)]^2 = [\omega^h(\vec{q}, j)]^2 + 2\omega^h(\vec{q}, j)D(\vec{q}, jj, \Omega) , \tag{4}$$

where

$$D(\vec{q}, jj, \Omega) = \Delta(\vec{q}, jj, \Omega) - i\Gamma(\vec{q}, jj, \Omega) . \tag{5}$$

Detailed expressions for the self-energy $D(\vec{q}, jj', \Omega)$ have been evaluated by a number of authors.[1,2,13,14] To second order in both cubic and quartic anharmonicity, the real part of the total anharmonic self-energy may be written

$$\Delta(\vec{q}, jj', \Omega) = \Delta^E(\vec{q}, jj') + \Delta^A(\vec{q}, jj', \Omega) , \tag{6}$$

where $\Delta^E(\vec{q}, jj')$ is the thermal-strain contribution given by

$$\Delta^E(\vec{q}, jj') = \frac{2}{\hbar} \sum V_{\alpha\beta}(\vec{q}j; -\vec{q}j')u^T_{\alpha\beta} , \tag{7}$$

and $\Delta^T(\vec{q}, jj', \Omega)$ is the anharmonic self-energy contribution given by

$$\Delta^A(\vec{q}, jj', \Omega) = \Delta^A(\vec{q}, jj') + \tilde{\Delta}^A(\vec{q}, jj', \Omega) , \tag{8}$$

where $\Delta^A(\vec{q},jj')$ is a frequency-independent contribution and $\tilde{\Delta}^A(\vec{q},jj',\Omega)$ is a frequency-dependent contribution to $\Delta^A(\vec{q},jj',\Omega)$ given by

$$\Delta^A(\vec{q},jj') = \Delta^{(4)}(\vec{q},jj') + \Delta^{(8)}(\vec{q},jj'), \tag{9}$$

with

$$\Delta^{(4)}(\vec{q},jj') = \frac{12}{\hbar}\sum_{\vec{q}_1 j_1} V(\vec{q}j;\vec{q}j';\vec{q}_1 j_1;-\vec{q}_1 j_1)(2n_1+1), \tag{10}$$

$$\Delta^{(8)}(\vec{q},jj') = -\frac{144}{\hbar^2}\sum_{\vec{q}_1 j_1}\sum_{j_2}\sum_{\vec{q}_3 j_3} V(\vec{q}j;\vec{q}j';-\vec{q}_1 j_1;-\vec{q}_1 j_2)\,V(\vec{q}_1 j_1;-\vec{q}_1 j_2;\vec{q}_3 j_3;-\vec{q}_3 j_3) \times\left(\frac{n_1+n_2+1}{\omega_1^h+\omega_2^h}-\frac{n_1-n_2}{\omega_1^h-\omega_2^h}\right)(2n_3+1), \tag{11}$$

and

$$\tilde{\Delta}^A(\vec{q},jj',\Omega) = \Delta^{(6)}(\vec{q},jj',\Omega) + \Delta^{(8)}(\vec{q},jj',\Omega), \tag{12}$$

with

$$\Delta^{(6)}(\vec{q},jj',\Omega) = -\frac{18}{\hbar^2}\sum_{\vec{q}_1 j_1}\sum_{j_2} |V(\vec{q}j;\vec{q}_1 j_1;-\vec{q}_1 j_2)|^2 R(\Omega), \tag{13}$$

$$\Delta^{(8)}(\vec{q},jj',\Omega) = -\frac{96}{\hbar^2}\sum_{\vec{q}_1 j_1}\sum_{\vec{q}_2 j_2}\sum_{\vec{q}_3 j_3} |V(\vec{q}j;\vec{q}_1 j_1;\vec{q}_2 j_2;\vec{q}_3 j_3)|^2 S(\Omega), \tag{14}$$

where

$$R(\Omega) = \left(\frac{n_1+n_2+1}{\Omega+\omega_1^h+\omega_2^h}-\frac{n_1+n_2+1}{\Omega-\omega_1^h-\omega_2^h}+\frac{2(n_1-n_2)}{\Omega-\omega_1^h+\omega_2^h}\right), \tag{15}$$

$$S(\Omega) = \left[\left([(n_1+1)(n_2+1)(n_3+1)-n_1n_2n_3]\left(\frac{1}{\Omega+\omega_1^h+\omega_2^h+\omega_3^h}-\frac{1}{\Omega-\omega_1^h-\omega_2^h-\omega_3^h}\right)\right.\right. + \left.\left.3[n_1(n_2+1)(n_3+1)-(n_1+1)n_2n_3]\left(\frac{1}{\Omega-\omega_1^h+\omega_2^h+\omega_3^h}-\frac{1}{\Omega+\omega_1^h-\omega_2^h-\omega_3^h}\right)\right)\right]. \tag{16}$$

The imaginary part of the self-energy is given by

$$\Gamma(\vec{q},jj',\Omega) = \Gamma^{(6)}(\vec{q},jj',\Omega) + \Gamma^{(8)}(\vec{q},jj',\Omega), \tag{17}$$

where

$$\tilde{\Delta}^A(\vec{q},jj',\Omega) = \frac{1}{\pi}\int_{-\infty}^{\infty}\frac{\Gamma(\vec{q},jj',\Omega)}{(\Omega-\Omega')_P}\,d\Omega'. \tag{18}$$

In these equations the n's are phonon population numbers, the V coefficients are the Fourier-transformed anharmonic force constants, and the superscripts on the Δ and Γ label that part of the quantity coming from the contributions to that order in parameter η when the Hamiltonian is of the form

$$H = H_0 + \eta^3 H_3 + \eta^4 H_4. \tag{19}$$

In this paper we shall be concerned with the quantities defined by Eqs. (5)–(18) evaluated at $\vec{q}\approx 0$ and with $j=j'=t$, the transverse-optic branch.

B. Numerical calculations

Numerical estimates of the different contributions to the real and imaginary parts of the anharmonic self-energy can be made provided the harmonic frequencies $\omega^h(\vec{q},j)$ are known throughout the Brillouin zone and provided a determination can be made of the complicated form of the V coefficients. For simple crystals like the alkali halides, reasonable lattice-dynamical calculations of the dispersion curves throughout the Brillouin zone can be made thus generating the eigenvectors and eigenvalues necessary for the evaluation of the lattice sums contained in Eqs. (7)–(17). An exact determination of the Fourier-transformed anharmonic force constants V is extremely difficult. If we follow Peierls[15] and rewrite the V as

$$V(\vec{q}_1 j_1;\ldots;\vec{q}_s j_s) = \tfrac{1}{2}(1/S!)(\hbar/2N)^{s/2}N\Delta(\vec{q}_1+\cdots+\vec{q}_s) \times[\omega_{j_1}(\vec{q}_1)\cdots\omega_{j_s}(\vec{q}_s)]^{1/2}C(\vec{q}_1 j_1;\ldots;\vec{q}_s j_s), \tag{20}$$

then Ipatova *et al.*[3] have argued that the C should have a constant order of magnitude for all values

of their arguments and that, as a first approximation, they may be replaced by constants [i.e., $|C_3|^2 = |C(0,j;\vec{q}_1 j_1; -\vec{q}_1 j_2)|^2$, etc.]. If the anharmonicity associated with the Coulomb forces is neglected, then these constants are simply, but tediously, related to various derivatives of the short-range repulsive energy as[3]

$$|C_3|^2 = \frac{16}{\omega^h(0,t)^2 S_3'} \frac{M_+ + M_-}{M_+^2 M_-^2} (r_0^6 B^2 + 6r_0^4 BC + 15r_0^2 C^2), \tag{21}$$

$$|C_4|^2 = \frac{4}{\omega^h(0,t)^2 S_4} \frac{(M_+ + M_-)^2}{M_+^3 M_-^3} \left(\frac{1}{M_+ M_-} \frac{M_+^3 + M_-^3}{M_+ + M_-} [4r_0^8 A^2 + 24 r_0^4 A(2r_0^2 B + 3C) + 60(4r_0^4 B^2 + 12 r_0^2 BC + 9C^2)] \right.$$
$$\left. + 3[2r_0^8 A^2 + 12 r_0^4 A(2r_0^2 B + C) + 6(16 r_0^4 B^2 + 20 r_0^2 BC + 15C^2)] \right), \tag{22}$$

$$C_4' = \frac{2}{3} \frac{1}{\omega^h(0,t)^2 \mu_2} \left(\frac{1}{M_+} + \frac{1}{M_-} \right)^2 (r_0^4 A + 10 r_0^2 B + 15C), \tag{23}$$

$$|C_4''|^2 = \frac{8}{3} \frac{1}{\omega^h(0,t)^2 \mu_2 S_2} \frac{(M_+ + M_-)^2}{M_+^3 M_-^3} \left(\frac{M_+^2 + M_-^2}{M_+ M_-} (r_0^4 A + 10 r_0^2 B + 15C)^2 \right.$$
$$\left. + [(r_0^4 A + 7 r_0^2 B)(r_0^4 A + 8 r_0^2 B + 5C) + (r_0^2 B + 5C)(r_0^4 A + 10 r_0^2 B + 15C)] \right), \tag{24}$$

where

$$A = (1/r_0^4)[\varphi^{IV}(r_0) - (6/r_0)\varphi^{III}(r_0) + (15/r_0^2)\varphi^{III}(r_0) - (15/r_0^3)\varphi^{I}(r_0)], \tag{25}$$

$$B = (1/r_0^3)[\varphi^{III}(r_0) - (3/r_0)\varphi^{II}(r_0) + (3/r_0^2)\varphi^{I}(r_0)], \tag{26}$$

$$C = (1/r_0^2)[\varphi^{II}(r_0) - (1/r_0)\varphi^{I}(r_0)], \tag{27}$$

$$\mu_2 = \frac{1}{6N} \sum_{\vec{q} j} [\omega^h(\vec{q}, j)]^2, \tag{28}$$

$$S_3 = \frac{1}{N} \sum_{\vec{q}} \sum_{jj'} [\omega^h(\vec{q}, j)]^2 [\omega^h(\vec{q}, j')]^2, \tag{29}$$

$$S_3' = \frac{1}{N} \sum_{\vec{q}} {\sum_{jj'}}' [\omega^h(\vec{q}, j)]^2 [\omega^h(\vec{q}, j')]^2, \tag{30}$$

$$S_4 = \frac{1}{N^2} \sum_{\vec{q}_1 \vec{q}_2 \vec{q}_3} \sum_{j_1 j_2 j_3} \Delta(\vec{q}_1 + \vec{q}_2 + \vec{q}_3)[\omega^h(\vec{q}, j_1)]^2 \times [\omega^h(\vec{q}, j_2)]^2 [\omega^h(\vec{q}_3, j_3)]^2, \tag{31}$$

with φ being the short-range repulsive force acting between nearest neighbors separated by r_0 and M_+ and M_- the ionic masses.

If the coefficients $C(\vec{q}_1 j_1; \ldots; \vec{q}_2 j_2)$ are really constants, then the relations $|C_4|^2 = |C_4'|^2 = |C_4''|^2$ should hold. Table I summarizes values of these constants for all the alkali halides discussed here. The data reveal that $|C_4'|^2$ is in fact reasonably close to $|C_4|^2$ for all the alkali halides. $|C_4''|^2$, however, deviates from this equality, being generally only about 20% of $|C_4'|^2$. Whether this difference in magnitude of $|C_4'|^2$ and $|C_4''|^2$ affects the calculation of the anharmonic self-energies in a significant way has been tested by Ipatova *et al.*[3] for lithium fluoride and sodium chloride. They report that an exact calculation of the V force constants leads to final results for the anharmonic self-energies which are not significantly different from these approximate estimates and because of this we have made the present calculations within the framework of the above approximation.

In calculating the principal parts and δ functions occurring in Eqs. (7)–(17) we have used the representation method suggested by Maradudin and Fein,[1] which involves the approximation

$$[(x)_P]^{-1} - i\pi\delta(x) = (x + i\epsilon)^{-1}, \tag{32}$$

where ϵ has a small but finite value. In the calculations to be presented we have used a mesh of 8000 points in the Brillouin zone for $\Gamma^{(6)}(0,t,\Omega)$ and $\Delta^{(6)}(0,t,\Omega)$, but only a mesh of 1000 points for the lengthier calculations of $\Gamma^{(8)}(0,t,\Omega)$ and $\Delta^{(8)}(0,t,\Omega)$. In general, a value of $\epsilon = 0.01\omega_L$ was used, where ω_L is the maximum frequency in the Brillouin zone.

Following the above procedures we have made numerical calculations of $\Delta^A(0,t,\Omega)$ and $\Gamma(0,t,\Omega)$ and their individual components for all of the alkali halides crystallizing in the NaCl structure. The harmonic eigenfrequencies used in these calculations have been generated via either the breathing shell model[16] or via the deformation dipole model incorporating next-nearest-neighbor interactions and a kind of three-body interaction.[17] The choice of lattice-dynamical model was determined by the closest fit to the available inelastic neutron scattering measurements of dispersion curves; in the absence of experimental dispersion curves, the lattice-dynamical results from the breathing shell model were used in the anharmon-

TABLE I. Values of the quantities that arise in the anharmonic calculations for (a) the lithium and sodium halides, and (b) the potassium and rubidium halides.

		LiF	LiCl	LiBr	LiI	NaF	NaCl	NaBr	NaI
A	(10^{51} erg cm^{-8})	99.474	16.782	9.688	4.576	43.682	9.4396	6.3861	3.6874
$-B$	(10^{35} erg cm^{-6})	38.403	9.384	6.101	3.367	19.684	5.885	4.302	2.774
C	(10^{19} erg cm^{-4})	16.862	5.865	4.286	2.747	9.8944	4.0569	3.1899	2.2846
μ_2	(10^{27} sec^{-2})	5.1327	1.8416	1.1985	0.7755	2.0669	0.8828	0.5769	0.3993
S_3	(10^{55} sec^{-4})	9.5457	1.2317	0.5261	0.2224	1.5392	0.2809	0.1199	0.0575
S_3'	(10^{56} sec^{-4})	7.1516	0.8778	0.3423	0.1348	1.1992	0.2174	0.0884	0.0411
S_4	(10^{84} sec^{-6})	29.194	1.349	0.872	0.098	1.9074	0.1486	0.0415	0.0138
$\lvert C_3\rvert^2$	(10^{12} erg^{-1})	0.9873	2.1245	1.9474	2.9969	0.8417	1.2027	1.1739	1.3761
$\lvert C_4\rvert^2$	(10^{25} erg^{-2})	0.1955	1.2639	2.8900	9.0489	0.1355	0.2799	0.4987	1.0519
$\lvert C_4'\rvert^2$	(10^{25} erg^{-2})	0.2350	1.6486	3.1259	12.002	0.2065	0.4768	0.7625	1.5670
$\lvert C_4''\rvert^2$	(10^{24} erg^{-2})	0.2839	2.510	5.236	17.745	0.3889	0.9421	1.5647	3.3734
ω_L	(cm^{-1})	674	480	430	371	434	271	225	201
		KF	KCl	KBr	KI	RbF	RbCl	RbBr	RbI
A	(10^{51} erg cm^{-8})	16.4083	4.6040	3.5312	1.7166	11.9852	4.560 85	2.8119	1.7695
$-B$	(10^{35} erg cm^{-6})	8.9896	3.2968	2.6515	1.5269	6.9484	3.0830	2.1959	1.5166
C	(10^{19} erg cm^{-4})	5.4291	2.5847	2.1695	1.4854	4.4124	2.3630	1.8604	1.4052
μ_2	(10^{27} sec^{-2})	1.1457	0.5657	0.3749	0.2756	0.7677	0.3989	0.2176	0.1547
S_3	(10^{55} sec^{-4})	4.7300	1.1523	0.5062	0.2735	2.1360	0.5731	0.1712	0.0865
S_3'	(10^{55} sec^{-4})	3.634	0.8968	0.3819	0.1988	1.5509	0.4383	0.1330	0.0663
S_4	(10^{82} sec^{-6})	32.485	3.9104	1.1378	0.4522	9.7814	1.3713	0.2251	0.0809
$\lvert C_3\rvert^2$	(10^{12} erg^{-1})	1.1648	1.1414	1.1052	0.7222	1.3374	1.3341	1.4025	1.3792
$\lvert C_4\rvert^2$	(10^{25} erg^{-2})	0.3044	0.2774	0.3451	0.2880	0.7307	0.5176	0.4022	0.4517
$\lvert C_4'\rvert^2$	(10^{25} erg^{-2})	0.5341	0.5454	0.6864	0.4393	1.2501	1.1155	0.9465	1.0571
$\lvert C_4''\rvert^2$	(10^{24} erg^{-2})	1.0380	1.1677	1.4720	1.0453	2.3897	2.3473	2.0012	2.3290
ω_L	(cm^{-1})	334	216	169	145	286	181	130	107

ic calculations. Values of the quantities that arise in the anharmonic calculations are summarized in Table I.

C. Results

Figure 1 shows the frequency dependence calculated for the different contributions to $\tilde{\Delta}^A(0,t,\Omega)$ and $\Gamma(0,t,\Omega)$ for NaBr, and Fig. 2 shows the calculated frequency dependence of $\Delta^A(0,t,\Omega)$ for NaBr at different temperatures. Such results are generally typical for all of the alkali halides crystallizing in the NaCl structure. Since at the present time experimental measurements of the total real or imaginary self-energy terms have been made only for $\Omega=0$ and $\Omega=\omega_t$, where ω_t is the quasinormal $q\approx 0$ transverse-optic-mode frequency, we shall confine our attention in this a paper to the anharmonic self-energies at these two frequencies rather than to the full frequency dependence.

Tables II–V summarize our calculated results for $\Delta^B(0,t)$, $\Delta^A(0,t,0)$, $\Delta^A(0,t,\omega_t)$, and $\Gamma(0,t,\omega_t)$ and their component contributions for the lithium, sodium, potassium, and rubidium halides, respectively. The data for $\Delta^A(0,t,\omega_t)$ and $\Gamma(0,t,\omega_t)$ and their respective components are given for the calculated value of ω_t which was determined from Eq. (4) using the appropriate values of $\omega^h(0,t)$ and $\Delta(0,t,\Omega)$ [see Fig. 2(a)].

An analysis of the data in Tables II–V reveals a number of overall qualitative features which should be commented on:

(i) The frequency-independent contribution $\Delta^A(0,t)$ is always dominated by the positive contributions from the first-order quartic term $\Delta^{(4)}(0,t)$; $\Delta^{(8)}(0,t)$ is always less than 10% of $\Delta^{(4)}(0,t)$ even above the characteristic Debye temperature.

(ii) $\tilde{\Delta}^A(0,t,0)$ is always dominated by the negative second-order cubic term $\Delta^{(6)}(0,t,0)$. Although $\Delta^{(8)}(0,t,0)$ is generally less than 10% of $\tilde{\Delta}^A(0,t,0)$ at low temperatures, it has a much stronger temperature dependence and can be as much as 30% of $\tilde{\Delta}^A(0,t,0)$ at the characteristic Debye temperature.

(iii) $\Delta^A(0,t,0)$ is always positive at low temperatures because of the dominance of the first-order quartic term $\Delta^{(4)}(0,t)$, but this usually becomes negative at higher temperatures because of the stronger temperature dependence of the negative

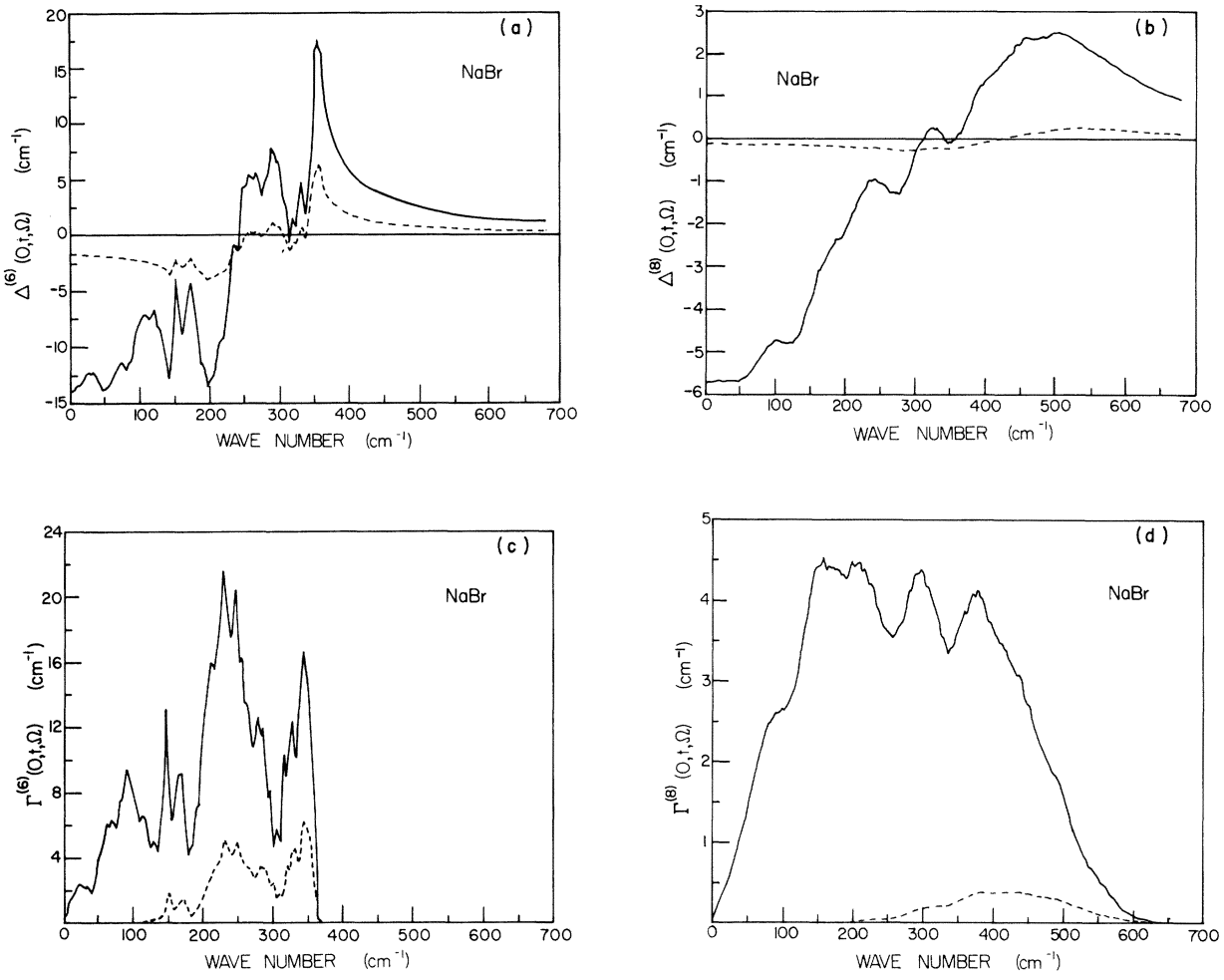

FIG. 1. Calculated frequency dependence at 5 K (dashed line) and 300 K (solid line) of (a) $\Delta^{(6)}(0,t,\Omega)$, (b) $\Delta^{(8)}(0,t,\Omega)$, (c) $\Gamma^{(6)}(0,t,\Omega)$, and (d) $\Gamma^{(8)}(0,t,\Omega)$ for NaBr.

contributions of $\Delta^{(6)}(0,t,0)$, $\Delta^{(8)}(0,t)$, and $\Delta^{(8)}(0,t,0)$.

(iv) $\tilde{\Delta}^{A}(0,t,\omega_t)$ is always dominated by the negative second-order cubic term $\Delta^{(6)}(0,t,\omega_t)$. At low temperatures $\Delta^{(8)}(0,t,\omega_t)$ is always less than 10% of $\tilde{\Delta}^{A}(0,t,\omega_t)$ but because of a strong temperature dependence it can be as much as 40% of $\tilde{\Delta}^{A}(0,t,\omega_t)$ at the characteristic Debye temperature.

(v) $\Delta^{A}(0,t,\omega_t)$ can be either positive or negative at low temperatures depending on the balance between $\Delta^{(4)}(0,t)$ and $\Delta^{(6)}(0,t,\omega_t)$. At higher temperatures $\Delta^{A}(0,t,\omega_t)$ is generally negative, however, because of the stronger temperature dependence of the negative contributions from $\Delta^{(6)}(0,t,\omega_t)$, $\Delta^{(8)}(0,t,\omega_t)$, and $\Delta^{(8)}(0,t)$.

(vi) $\Gamma(0,t,\omega_t)$ is totally determined at low temperatures by the second-order cubic terms, $\Gamma^{(6)}(0,t,\omega_t)$. However, $\Gamma^{(8)}(0,t,\omega_t)$ has a much stronger temperature dependence than $\Gamma^{(6)}(0,t,\omega_t)$ and both contributions to $\Gamma(0,t,\omega_t)$ are generally very close in magnitude at the characteristic Debye temperature.

III. EXPERIMENT

A. Introduction

In Sec. II it was shown that the quasinormal frequency measured in any resonance experiment is given by

$$[\omega_{T,0}(0,t)]^2=[\omega^h(0,t)]^2 + 2\omega^h[\Delta_T^A(0,t,\omega_t)+\Delta^E(0,t)] \quad (33)$$

for an applied frequency $\Omega=\omega_t\equiv\omega_{T,0}(0,t)$, where the subscripts $T,0$ in $[\omega_{T,0}(0,t)]^2$ denote the temperature and (zero) pressure, respectively, and where the subscript T has now been added to the anharmonic self-energy to denote the temperature. At the same temperature T, but at an applied pressure P which is such as to reduce the volume to

TABLE II. Calculated values, in cm^{-1}, of the different contributions to $\Delta^E(0,t)$, $\Delta^A(0,t,0)$, $\Delta^A(0,t,\omega_t)$, and $\Gamma(0,t,\omega_t)$ for the lithium halides.

	LiF				LiCl				LiBr				LiI		
Temperature (K)	5	100	300	500	5	100	200	300	5	100	200	300	5	100	200
$\omega(0,t)$	316.9	316.3	300.8	278.7	220.3	214.8	192.1	153.4	191.5	179.0	146.6	173.0	147.7	127.2	146.0
$\Delta^E(0,t)$	0	−0.6	−10.9	−26.4	0	−4.1	−20.2	−40.8	0	−6.7	−26.7	−50.5	0	−12.8	−43.4
$\Delta^{(4)}(0,t)$	13.0	13.3	19.1	27.7	14.1	16.0	22.4	30.6	12.5	16.1	24.6	34.6	14.5	21.4	35.2
$\Delta^{(8)}(0,t)$	−0.2	−0.2	−0.7	−1.6	−0.4	−0.7	−1.7	−3.6	−0.4	−0.9	−2.9	−6.0	−0.5	−2.2	−7.1
$\Delta^A(0,t)$	12.8	13.1	18.4	26.1	13.7	15.3	20.7	27.0	12.1	15.1	21.8	28.5	13.9	19.2	28.0
$\Delta^{(6)}(0,t,0)$	−9.8	−11.1	−25.2	−41.7	−8.4	−13.3	−25.2	−37.6	−4.6	−10.0	−19.6	−29.4	−5.3	−15.2	−30.0
$\Delta^{(8)}(0,t,0)$	−1.1	−1.2	−5.0	−13.6	−1.6	−3.1	−10.0	−22.0	−1.7	−5.3	−19.1	−42.7	−2.3	−11.8	−45.2
$\tilde{\Delta}^A(0,t,0)$	−10.9	−12.3	−30.3	−55.3	−10.0	−16.4	−35.1	−59.6	−6.4	−15.3	−38.7	−72.1	−7.5	−27.0	−75.3
$\Delta^A(0,t,0)$	2.0	0.8	−11.8	−29.2	3.7	−1.1	−14.4	−32.5	5.8	−0.3	−17.0	−43.6	6.4	−7.9	−47.2
$\Delta^{(6)}(0,t,\omega_t)$	−12.7	−13.1	−19.1	−27.1	−12.7	−14.3	−18.9	−23.1	−5.1	−9.5	−13.8	−25.4	−5.7	−5.6	−11.7
$\Delta^{(8)}(0,t,\omega_t)$	−1.2	−1.4	−5.0	−13.3	−1.9	−3.2	−9.0	−21.0	−2.1	−6.0	−17.6	−43.4	−2.8	−13.6	−47.9
$\tilde{\Delta}^A(0,t,\omega_t)$	−13.9	−14.4	−24.1	−40.4	−14.5	−17.5	−28.0	−44.1	−7.2	−15.5	−31.5	−68.8	−8.4	−19.3	−59.7
$\Delta^A(0,t,\omega_t)$	−1.1	−1.3	−5.7	−14.3	−0.8	−2.2	−7.3	−17.1	4.9	−0.4	−9.7	−40.3	5.5	−0.1	−31.6
$\Gamma^{(6)}(0,t,\omega_t)$	0.3	0.7	6.1	9.3	0.8	2.2	5.4	9.6	4.1	7.8	7.4	18.6	0.02	11.4	6.9
$\Gamma^{(8)}(0,t,\omega_t)$	0	0.1	2.4	7.2	0	1.0	5.1	9.9	0	2.7	4.9	25.0	0.12	3.7	40.1
$\Gamma(0,t,\omega_t)$	0.3	0.8	8.4	16.5	0.8	3.2	10.5	19.6	4.1	10.1	12.2	43.6	0.14	15.1	47.0

TABLE III. Calculated values, in cm^{-1}, of the different contributions to $\Delta^E(0,t)$, $\Delta^A(0,t,0)$, $\Delta^A(0,t,\omega_t)$, and $\Gamma(0,t,\omega_t)$ for the sodium halides.

	NaF				NaCl				NaBr				NaI			
Temperature (K)	5	100	200	300	5	100	200	300	5	100	200	300	5	100	200	300
$\omega(0,t)$	255	254	248	239	174	171	164	154	143	140	133	124	123	120	110	92.5
$\Delta^E(0,t)$	0	−0.63	−3.69	−7.79	0	−1.09	−4.56	−8.61	0	−1.39	−4.97	−8.98	0	−1.78	-5.90	−10.38
$\Delta^{(4)}(0,t)$	5.44	7.17	9.55	12.95	3.93	5.81	8.98	12.95	3.27	5.13	8.96	13.02	3.43	6.05	10.60	15.10
$\Delta^{(8)}(0,t)$	−0.08	−0.13	−0.32	−0.65	−0.06	−0.15	−0.47	−1.01	−0.05	−0.19	−0.62	−1.36	−0.06	−0.32	−1.12	−2.46
$\Delta^A(0,t)$	5.36	7.04	9.23	12.30	3.87	5.66	8.51	11.94	3.22	4.94	8.34	11.66	3.37	5.73	9.48	12.64
$\Delta^{(6)}(0,t,0)$	−4.49	−6.42	−11.86	−17.71	−2.82	−5.79	−11.37	−17.04	−1.69	−4.59	−9.10	−13.65	−1.32	−4.57	−9.12	−13.69
$\Delta^{(8)}(0,t,0)$	−0.26	−0.42	−1.27	−2.79	−0.15	−0.47	−1.74	−3.90	−0.13	−0.66	−2.54	−5.71	−0.15	−1.16	−4.56	−10.25
$\tilde{\Delta}^A(0,t,0)$	−4.76	−6.84	−13.13	−20.50	−2.97	−6.26	−13.11	−20.94	−1.82	−5.24	−11.64	−19.36	−1.47	−5.73	−13.68	−23.94
$\Delta^A(0,t,0)$	1.60	0.20	-3.90	−8.20	0.90	−0.61	−4.60	−9.00	1.41	−0.30	−3.30	−7.70	1.91	0	−4.20	−11.30
$\Delta^{(6)}(0,t,\omega_t)$	−6.65	−7.17	−9.20	−12.20	−4.38	−5.32	−7.77	−10.42	−3.40	−4.58	−5.88	−6.86	−1.47	−1.59	−3.03	−7.76
$\Delta^{(8)}(0,t,\omega_t)$	−0.30	−0.45	−1.10	−2.36	−0.18	−0.42	−1.36	−3.17	−0.16	−0.60	−2.09	−4.75	−0.19	−1.11	−4.33	−8.45
$\tilde{\Delta}^A(0,t,\omega_t)$	−6.95	−7.62	−10.30	−14.56	−4.56	−5.75	−9.13	−13.59	−3.55	−5.17	−7.97	−11.61	−1.66	−2.70	−7.36	−16.21
$\Delta^A(0,t,\omega_t)$	−1.59	−0.58	−1.07	−2.26	−0.69	−0.09	−0.62	−1.65	−0.33	−0.23	0.37	0.06	1.71	3.03	2.12	−3.57
$\Gamma^{(6)}(0,t,\omega_t)$	0.20	0.54	1.23	2.36	0.27	0.86	1.41	2.55	0.69	1.74	3.19	5.08	0.72	2.97	7.37	11.38
$\Gamma^{(8)}(0,t,\omega_t)$	0	0.14	0.93	2.29	0	0.27	1.39	3.18	0	0.38	1.60	3.29	0	0.80	2.63	3.50
$\Gamma(0,t,\omega_t)$	0.20	0.67	2.16	4.65	0.27	1.14	2.80	5.74	0.69	2.12	4.79	8.37	0.73	3.77	10.00	14.89

TABLE IV. Calculated values, in cm^{-1}, of the different contributions to $\Delta^E(0,t)$, $\Delta^A(0,t,0)$, $\Delta^A(0,t,\omega_t)$, and $\Gamma(0,t,\omega_t)$ for the potassium halides.

	KF				KCl				KBr				KI			
Temperature (K)	5	100	200	300	5	100	200	300	5	100	200	300	5	100	200	300
$\omega(0,t)$	201.4	200.1	195.3	188.8	149.8	149.8	146.2	141.9	123.5	122.8	119.8	115.8	110.2	110.2	109.2	107.7
$\Delta^E(0,t)$	0	−1.09	−5.18	−10.19	0	−1.07	−4.04	−7.37	0	−1.15	−3.82	−6.72	0	−0.95	−2.91	−4.99
$\Delta^{(4)}(0,t)$	5.87	7.15	10.91	15.30	3.14	4.57	7.77	11.25	2.28	3.90	6.95	10.18	1.35	2.67	4.90	7.22
$\Delta^{(8)}(0,t)$	−0.09	−0.21	−0.61	−1.28	−0.04	−0.14	−0.48	−1.05	−0.02	−0.14	−0.48	−1.06	−0.01	−0.08	−0.30	−0.67
$\Delta^A(0,t)$	5.78	6.95	10.30	14.02	3.10	4.43	7.29	10.20	2.26	3.77	6.47	9.12	1.34	2.59	4.59	6.55
$\Delta^{(6)}(0,t,0)$	−3.47	−6.46	−12.55	−18.81	−1.80	−4.61	−9.16	−13.75	−1.10	−3.60	−7.17	−10.76	−0.51	−2.09	−4.18	−6.27
$\Delta^{(8)}(0,t,0)$	−0.24	−0.60	−2.15	−4.81	−0.08	−0.38	−1.46	−3.27	−0.05	−0.37	−1.48	−3.32	−0.03	−0.28	−1.10	−2.47
$\tilde{\Delta}^A(0,t,0)$	−3.71	−7.06	−14.70	−23.62	−1.89	−4.99	−10.62	−17.02	−1.15	−3.97	−8.65	−14.08	−0.53	−2.37	−5.28	−8.74
$\Delta^A(0,t,0)$	2.07	−0.12	−4.41	−9.59	1.21	−0.56	−3.33	−6.82	1.11	−0.21	−2.20	−4.97	0.81	0.22	−0.68	−2.19
$\Delta^{(6)}(0,t,\omega_t)$	−5.63	−6.69	−9.43	−12.27	−3.08	−4.27	−6.95	−9.44	−1.69	−2.48	−4.70	−6.98	−0.65	−0.70	−1.09	−1.35
$\Delta^{(8)}(0,t,\omega_t)$	−0.29	−0.59	−1.75	−3.90	−0.10	−0.29	−0.95	−2.20	−0.06	−0.30	−1.06	−2.40	−0.03	−0.24	−0.90	−2.04
$\tilde{\Delta}^A(0,t,\omega_t)$	−5.91	−7.28	−11.18	−16.17	−3.18	−4.56	−7.90	−11.64	−1.76	−2.77	−5.76	−9.38	−0.68	−0.94	−1.99	−3.39
$\Delta^A(0,t,\omega_t)$	−0.13	−0.33	−0.89	−2.14	−0.08	−0.13	−0.61	−1.43	0.50	0.99	0.71	−0.26	0.66	1.65	2.60	3.15
$\Gamma^{(6)}(0,t,\omega_t)$	0.47	0.93	1.90	3.13	0.18	0.51	1.33	1.91	0.60	1.77	3.10	4.10	0.19	0.68	1.44	1.89
$\Gamma^{(8)}(0,t,\omega_t)$	0	0.33	1.73	3.90	0	0.28	1.29	2.93	0	0.26	1.11	2.47	0	0.23	0.97	2.12
$\Gamma(0,t,\omega_t)$	0.47	1.26	3.63	7.04	0.18	0.78	2.62	4.84	0.60	2.03	4.22	6.57	0.19	0.91	2.41	4.01

TABLE V. Calculated values, in cm^{-1}, of the different contributions to $\Delta^E(0,t)$, $\Delta^A(0,t,0)$, $\Delta^A(0,t,\omega_t)$, and $\Gamma(0,t,\omega_t)$ for the rubidium halides.

	RbF				RbCl				RbBr				RbI			
Temperature (K)	5	100	200	300	5	100	200	300	5	100	200	300	5	100	200	300
$\omega(0,t)$	164.3	161.9	154.4	145.6	126.1	124.3	120.3	114.7	94.55	93.12	90.0	86.55	81.67	80.54	78.04	75.15
$\Delta^E(0,t)$	0	−2.03	−7.51	−13.76	0	−1.61	−5.25	−9.20	0	−1.33	−3.88	−6.55	0	−1.29	−3.55	−5.88
$\Delta^{(4)}(0,t)$	5.77	7.97	13.03	18.65	3.11	5.16	9.14	13.36	1.60	3.31	6.16	9.11	1.22	2.94	5.57	8.27
$\Delta^{(8)}(0,t)$	−0.11	−0.34	−1.10	−2.35	−0.04	−0.23	−0.80	−1.75	−0.02	−0.13	−0.50	−1.10	−0.01	−0.13	−0.49	−1.10
$\Delta^A(0,t)$	5.66	7.63	11.93	16.30	3.07	4.93	8.34	11.61	1.59	3.18	5.66	8.01	1.21	2.81	5.08	7.17
$\Delta^{(6)}(0,t,0)$	−2.43	−5.83	−11.43	−17.12	−1.43	−4.49	−8.97	−13.46	−0.85	−3.53	−7.06	−10.60	−0.60	−2.98	−5.96	−8.94
$\Delta^{(8)}(0,t,0)$	−0.28	−1.10	−4.18	−9.37	−0.09	−0.58	−2.27	−5.11	−0.03	−0.33	−1.32	−2.97	−0.02	−0.32	−1.28	−2.88
$\tilde{\Delta}^A(0,t,0)$	−2.71	−6.92	−15.61	−26.49	−1.51	−5.07	−11.24	−18.57	−0.88	−3.86	−8.38	−13.57	−0.62	−3.30	−7.24	−11.82
$\Delta^A(0,t,0)$	2.95	0.71	−3.68	−10.19	1.55	−0.14	−2.90	−6.96	0.70	−0.68	−2.72	−5.56	0.60	−0.50	−2.16	−4.65
$\Delta^{(6)}(0,t,\omega_t)$	−3.99	−5.38	−8.47	−10.70	−2.79	−4.42	−6.72	−8.68	−1.49	−2.97	−5.34	−6.97	−1.00	−2.24	−4.06	−5.38
$\Delta^{(8)}(0,t,\omega_t)$	−0.34	−1.29	−4.25	−8.24	−0.11	−0.51	−1.95	−4.49	−0.03	−0.22	−0.87	−2.10	−0.02	−0.22	−0.83	−1.99
$\tilde{\Delta}^A(0,t,\omega_t)$	−4.33	−6.67	−12.72	−18.94	−2.90	−4.93	−8.67	−13.18	−1.52	−3.19	−6.21	−9.07	−1.02	−2.46	−4.90	−7.38
$\Delta^A(0,t,\omega_t)$	1.33	0.96	−0.79	−2.64	0.17	0	−0.33	−1.57	0.06	−0.02	−0.54	−1.06	1.86	0.35	0.18	−0.20
$\Gamma^{(6)}(0,t,\omega_t)$	0.87	2.50	4.83	6.95	0.59	1.26	1.96	2.86	0.24	0.98	1.05	1.77	0.27	1.17	1.47	2.27
$\Gamma^{(8)}(0,t,\omega_t)$	0	0.72	2.24	4.62	0	0.46	1.88	3.65	0	0.28	1.17	2.58	0	0.26	1.07	2.32
$\Gamma(0,t,\omega_t)$	0.87	3.22	7.06	11.57	0.59	1.72	3.84	6.51	0.24	1.26	2.22	4.35	0.27	1.43	2.54	4.60

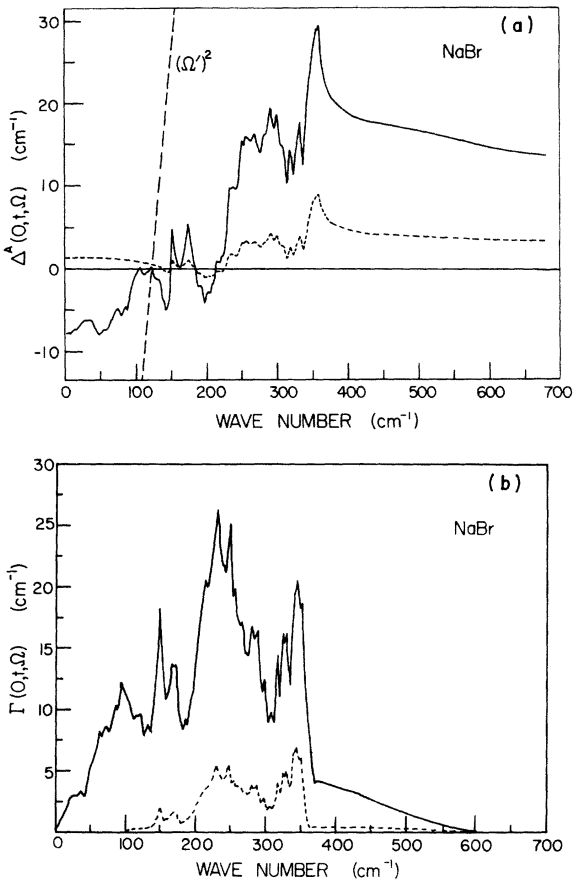

FIG. 2. Calculated frequency dependence at 5 K (dashed line) and 300 K (solid line) of (a) $\Delta^A(0,t,\Omega)$ and (b) $\Gamma(0,t,\Omega)$ for NaBr. Also shown in (a) is the line of Ω'^2, where

$$\Omega'^2 = \left(\frac{\Omega^2 - \{[\omega^h(0,t)]^2 + 2\omega^h(0,t)\Delta^E(0,t)\}}{2\omega^h(0,t)} \right)_{290\,\mathrm{K}} .$$

The intersection of the lines Ω'^2 and $\Delta^A_{290}(0,t,\Omega)$ gives the calculated quasinormal frequency, $\omega(0,t)$, in this case at 290 K.

that which the crystal has at 0 K and zero pressure, Eq. (33) becomes

$$[\omega_{T,P}(0,t)]^2 = [\omega^h(0,t)]^2 + 2\omega^h \Delta^A_T(0,t,\omega_t) . \quad (34)$$

This leads immediately to

$$\Delta^E(0,t) = -\{[\omega_{T,P}(0,t)]^2 - [\omega_{T,0}(0,t)]^2\}/2\omega^h(0,t) \quad (35)$$

or

$$\Delta^E(0,t) \approx -\{[\omega_{T,P}(0,t)]^2 - [\omega_{T,0}(0,t)]^2\}/2\omega_{0,0}(0,t) , \quad (36)$$

where

$$\omega^h(0,t) \approx \omega_{0,0}(0,t) . \quad (37)$$

Equation (36) therefore leads to a determination of the thermal-strain contribution $\Delta^E(0,t)$ from suitable experimental measurements.

$\Delta^A_T(0,t,\omega_t)$ is determined as follows. At $T=0$ K and at zero pressure, Eq. (33) becomes

$$[\omega_{0,0}(0,t)]^2 = [\omega^h(0,t)]^2 + 2\omega^h(0,t)\Delta^A_0(0,t,\omega'_t) , \quad (38)$$

where

$$\omega'_t = \omega_{00}(0,t) ,$$

while at a temperature T and a suitably chosen applied pressure P so as to maintain the crystal volume at that found for the crystal at 0 K and zero pressure, Eq. (33) becomes

$$[\omega_{T,P}(0,t)]^2 = [\omega^h(0,t)]^2 + 2\omega^h(0,t)\Delta^A_T(0,t,\omega_t) , \quad (39)$$

which leads to

$$\Delta^A_T(0,t,\omega_t) - \Delta^A_0(0,t,\omega'_t) = \{[\omega_{T,P}(0,t)]^2 - [\omega_{0,0}(0,t)]^2\}/2\omega^h(0,t) , \quad (40)$$

$$\approx \{[\omega_{T,P}(0,t)]^2 - [\omega_{0,0}(0,t)]^2\}/2\omega_{0,0}(0,t) \equiv -A'(T) . \quad (41)$$

Equation (41) therefore allows an experimental determination of the change in the anharmonic self-energy between a temperature T and 0 K via suitable studies of the temperature and pressure dependence of $\omega(0,t)$. $\Delta^A_0(0,t,\omega'_t)$ is not necessarily zero because anharmonic interactions can persist in the presence of zero-point fluctuations. However, experimental estimates of $\Delta^A_0(0,t,\omega'_t)$ can be made as follows. For temperatures close to the Debye temperature and above, it can be shown that the thermal population factors vary linearly with T and also that the leading terms in both the cubic and quartic anharmonic contributions to $\Delta^A_T(0,t,\omega_t)$ are linear in T. If such a linearity is found for $A'(T)$, therefore, extrapolations of these linear parts back to $T=0$ will yield an intercept of $\Delta^A_0(0,t,\omega'_t)$, and hence $\Delta^A_T(0,t,\omega_t)$ can be determined from Eq. (41).

B. Spectroscopic measurements

For simple ionic solids like the alkali and heavy-metal halides, the $q \approx 0$ optic modes are most conveniently studied via far-infrared spectroscopy. The $q \approx 0$ transverse-optic-mode frequencies and lifetimes are readily determined from suitable measurements of the normal incidence transmission spectra of thin films of the material under investigation. Electromagnetic analysis of thin-film behavior shows that the minimum in the spectral transmission for such a thin film occurs at

$\omega(0,t)$ providing the film is thin compared to the vacuum wavelength of the incident radiation.[18] A similar analysis reveals that $2\Gamma(0,t,\omega_t)$ is determined by the spectral damping measured at a transmission T', where T' is given by

$$T' = 2T_0/(1+T_0), \tag{42}$$

with T_0 being the transmission at $\omega(0,t)$. This procedure therefore allows a direct determination of $\omega(0,t)$ and $2\Gamma(0,t,\omega_t)$ without lengthy analysis of the data, as would be required to deduce these parameters from reflection data.

The far-infrared spectroscopic measurements were achieved using an R.I.I.C. FS-520 or FS-720 Michelson Fourier spectrophotometer used in conjunction with a Golay cell or gallium-doped germanium bolometer as a detector. Below 150 cm^{-1} a mercury-arc discharge tube was used as a source, but above 150 cm^{-1} a Nernst glower was utilized.

C. Low-temperature measurements

The low-temperature measurements of $\omega(0,t)$ were made with a metal cryostat, with the sample mounted on the base of the helium can, the full details of which have been described elsewhere.[19] Because many of the alkali halides were hygroscopic, an evaporation gun was therefore incorporated into the cryostat and the thin films of the more hygroscopic compounds were prepared *in situ* without exposing them to the atmosphere.[19]

D. High-pressure measurements

The requirements of hydrostatic pressure containment and far-infrared spectroscopy are somewhat conflicting. The first requires small apertures for maximum strength while the second requires large apertures to provide maximum energy throughput from the comparatively weak far-infrared sources. These requirements are further complicated because of the scarcity of readily available window materials which satisfy the competing demands of strength and transmissivity in the far infrared. As a result of these difficulties, much of the very limited far-infrared high-pressure research has been confined to date to work achieved with the opposed diamond anvil system.[20] When used properly this cell is a powerful tool in the very-high-pressure domain, but, in the important 0–10-kbar range involved in the present work, reliable far-infrared measurements are difficult to perform with this cell. This is primarily because of the difficulty in accurately determining the system operating pressure but also because of the inherent difficulty of achieving true hydrostatic pressure conditions because of residual pressure gradients across the anvil faces. The consequences of these problems have been that it is difficult to precisely determine the pressure dependence of mode eigenfrequencies, especially at the low pressures necessary for the evaluation of $\omega_{T,P}(0,t)$, and it is virtually impossible to reliably measure the (small) pressure dependence of the associated linewidths using the diamond anvil system.

Accordingly we have developed a high-pressure far-infrared cell which goes some way to solving these problems, and this is illustrated in Fig. 3. The cell body, window mounts, and retaining closures were machined from 4340 alloy steel and then heat treated to a hardness of RC45 giving a yield strength of 14 kbars. The critical bores and surfaces of the cell and its components were ground and honed to size after the hardening process. The cell body measures $17\times14\times10$ cm and fully assembled the cell has an effective speed of $f2.4$.

The window mounts used in the cell gave a supported to unsupported area ratio of about 3 with an unsupported port diameter of 5 mm. The window high-pressure seal was achieved by lapping and polishing the mating surfaces of the window and its mount to be flat and parallel to better than 300 Å. The windows were prevented from sliding off their mounts by brass retaining rings attached to the window mounts. The window mount pressure seal was achieved using a stainless-steel, brass, and Teflon packing assembly.

In choosing both the cell windows and the pressure transmission medium, care must be used to avoid materials which have characteristic electromagnetic resonances in the spectral region under investigation. The choice of materials available for both window and pressure transmission media for far-infrared service is extremely restricted however. For windows we have used $\frac{1}{4}$-in.-thick fused quartz for the spectral range below 125 cm^{-1} and $\frac{1}{2}$-in.-thick silicon for the spectral range 125–400 cm^{-1}. For a pressure transmission medium we have used either helium or argon gas since these exhibit no characteristic far-infrared resonances as do most of the organic oils and molecular gases conventionally used in high-pressure research.

Figure 4 shows the experimental arrangement for a high-pressure far-infrared transmission experiment. The high-pressure cell is located in an isolated evacuated thick-walled module B designed to protect the interferometric and detector modules A and C, respectively. The cell window axis is deliberately chosen to be off line with both the entrance and exit ports to module B to avoid any possible damage to the interferometer or detec-

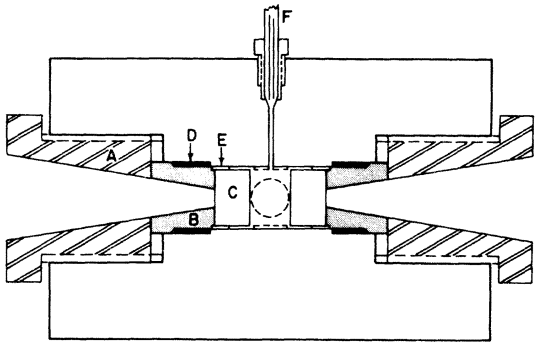

FIG. 3. High-pressure far-infrared cell. A, retaining closure; B, window mount; C, window; D, packing; E, window retaining ring; F, gas input line.

tor due to a high-pressure window failure.

The hydrostatic pressure for these experiments was generated from a two-stage gas compressor. The pressure was measured using a suitably aged and calibrated manganin cell. With this high-pressure spectroscopic arrangement we are able to make spectral studies in the far infrared under truly hydrostatic pressure conditions with a pressure accuracy of better than ± 1% whilst at the same time achieving signal-to-noise values of better than 50.

E. Sample preparation

The results given in Sec. III F were all obtained using thin-film samples evaporated on to Mylar or Teflon substrates using the highest-purity starting material available. Because of its hygroscopic nature, the NaBr samples used in the pressure experiments were overcoated with LiF to protect them from the atmosphere while they were being loaded into the cell. After being loaded into the cell, these samples yielded the same characteristic spectral parameters at zero pressure as for uncoated, unexposed samples. Similar procedures for some of the other hygroscopic alkali halides were unsuccessful, however. As mentioned earlier, all the samples used in the low-temperature experiments were prepared *in situ* within the cryostat.

We have critically examined the influence of film quality and choice of substrate on the measured characteristic spectral parameters. In general, film quality had little effect on $\omega(0,t)$ except that the transmission minimum could be displaced by 1 or 2% to higher frequencies when the crystallite size was large or when the films had become cracked because of excessive temperature or pressure cycling. Poor film quality, however, can cause significant increases in $2\Gamma(0,t,\omega_t)$ by as much as 50%. In general, the different organic substrates used had little effect on the spectral parameters.

In order to test the equivalence of our thin-film sample temperature data to that of bulk material, we also determined the characteristic spectral parameters for a few materials via Kramers-Kronig analyses of reflection data from bulk single crystals. In all cases the data were in close correspondence. In testing the equivalence of our thin-film pressure data to that of bulk material we have used the pressure-induced phase transition in RbBr. For bulk material this transition occurs at 5.75 kbar.[21] Figure 5 shows our measured pressure dependence of the spectral profile of the $q \approx 0$ transverse-optic mode for RbBr in both phases. As can be seen the profile is well defined in both phases and we observe the transition at 5.80 kbar.

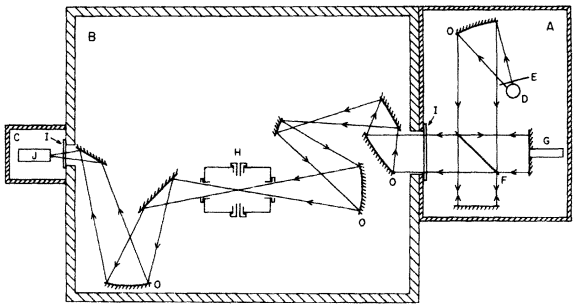

FIG. 4. High-pressure far-infrared transmission experiment. A, Michelson interferometric module; B, high-pressure cell module; C, detector module; D, source; E, chopper; F, beam splitter; G, moving mirror; H, high-pressure cell; I, module vacuum window; J, detector; O, mirrors.

F. Experimental results

Figure 6 shows the measured temperature and pressure dependence of $\omega(0,t)$ and $2\Gamma(0,t,\omega_t)$ for a few representative compounds and Tables VI and VII summarize the temperature and pressure dependence of $\omega(0,t)$ and $2\Gamma(0,t,\omega_t)$ for all the materials investigated.

The temperature dependence of $\omega(0,t)$ has been reported previously for a few of the compounds reported here.[22] Where overlap has occurred, there is generally a good agreement with the data for $\omega(0,t)$ reported here. The pressure measurements reveal that $\omega(0,t)$ has a linear dependence on pressure, for pressures up to about 7 kbar, for all the materials investigated. Values of $[d\omega(0,t)/dP]_T$ determined from least-squares fits to these data are summarized in Table VI and

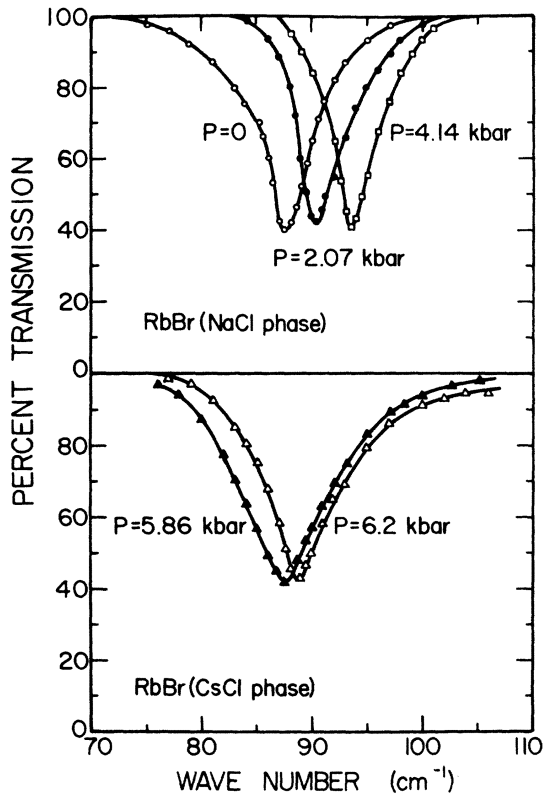

FIG. 5. Measured pressure dependence of the spectral profile of the $q \approx 0$ transverse-optic mode for RbBr in both the NaCl phase and the high-pressure CsCl phase. The NaCl→CsCl transformation was observed at 5.8 kbar.

from these data the mode Grüneisen parameters have been determined from the relation

$$\gamma_t = -\frac{1}{\beta_T}\left(\frac{1}{\omega(0,t)}\frac{d\omega(0,t)}{dP}\right)_T , \tag{43}$$

where β_T is the isothermal compressibility. The values used for β_T were determined from suitably corrected values of the adiabatic elastic constants.[23-34] The mode Grüneisen parameters are summarized in Table VI. Also shown in the table are mode Grüneisen parameters for a few compounds which have previously been reported from measurements with the diamond anvil cell.[9,35-38] With the exception of the values reported for the heavy-metal halides,[9] there is only a fair agreement with the present work where overlap has occurred. However, for the technical reasons cited earlier, we believe the present data to be significantly more accurate because of the genuine hydrostatic pressure environment that our samples have been subjected to and because of the greater accuracy in measuring our system operating pressure.

Our measurements of the temperature dependence of $2\Gamma(0, t, \omega_t)$ generally reveal a substantial decrease with decreasing temperature. Nevertheless, the linewidths at liquid-helium temperatures are still significant. Measurements of $2\Gamma(0, t, \omega_t)$ have previously been reported[22] for a few of the materials studied here and, although there is generally good agreement at 290 K between the two sets of data, it is to be noted that the present data show a much stronger temperature dependence, and consequently a much smaller damping, at liquid-helium temperatures than the earlier data.

The variation of the spectral damping with pressure was found to be small. The results of least-squares fits to determine $d2\Gamma(0, t, \omega_t)/dP$ are shown in Table VII and these reveal the damping to change by only a few percent per kilobar for most of the compounds. Because of the smallness of this dependence on pressure and because of the experimental error, the sign of the $d2\Gamma(0, t, \omega_t)/dP$ is only unambiguously determined for a few of the materials and even for these the data reveal that the $d2\Gamma(0, t, \omega_t)/dP$ can be either positive or negative.

G. Experimental self-energies

The temperature and pressure dependence of $\omega(0, t)$ reported in Sec. III F can be used to determine $\Delta_T^A(0, t, \omega_t)$ and $\Delta^E(0, t)$ as outlined in the introduction to this section. A room-temperature value of $\omega_{T,P}(0, t)$ can be directly determined from our measurements of the pressure dependence of $\omega(0, t)$, once the value of P in Eqs. (36) and (41) is known. In order to determine $\omega_{T,P}(0, t)$ below room temperature we note that Eq. (33) can be restated as

$$[\omega(0,t)]^2 = [\omega^E(0,t)]^2 + 2\omega^h(0,t)\Delta_T^A(0,t,\omega_t) , \tag{44}$$

where $\omega^E(0, t)$ is the quasiharmonic mode frequency given by

$$[\omega^E(0,t)]^2 = [\omega^h(0,t)]^2 + 2\omega^h(0,t)\Delta^E(0,t) \tag{45}$$

and is determined by volume alone and is not explicitly dependent on temperature. On the other hand, the first-order volume dependence of $\Delta_T^A(0, t, \omega_t)$ can arise only from the anharmonic force constants [see Eqs. (8)–(16)] and in the following discussion we show that this is small. Consequently $[\partial \ln\omega(0, t)/\partial \ln V]_T$ should not be very dependent explicitly on temperature and if we assume this to be the case then we can use our room-temperature measurements of $\omega(0, t)$ against pressure to determine $\omega_{T,P}(0, t)$ at any lower temperature. Preliminary measurements of γ_t at low temperatures support the adequacy of this approximation.

The values of the pressure P required to decrease the volume of the crystal at T (K) to that

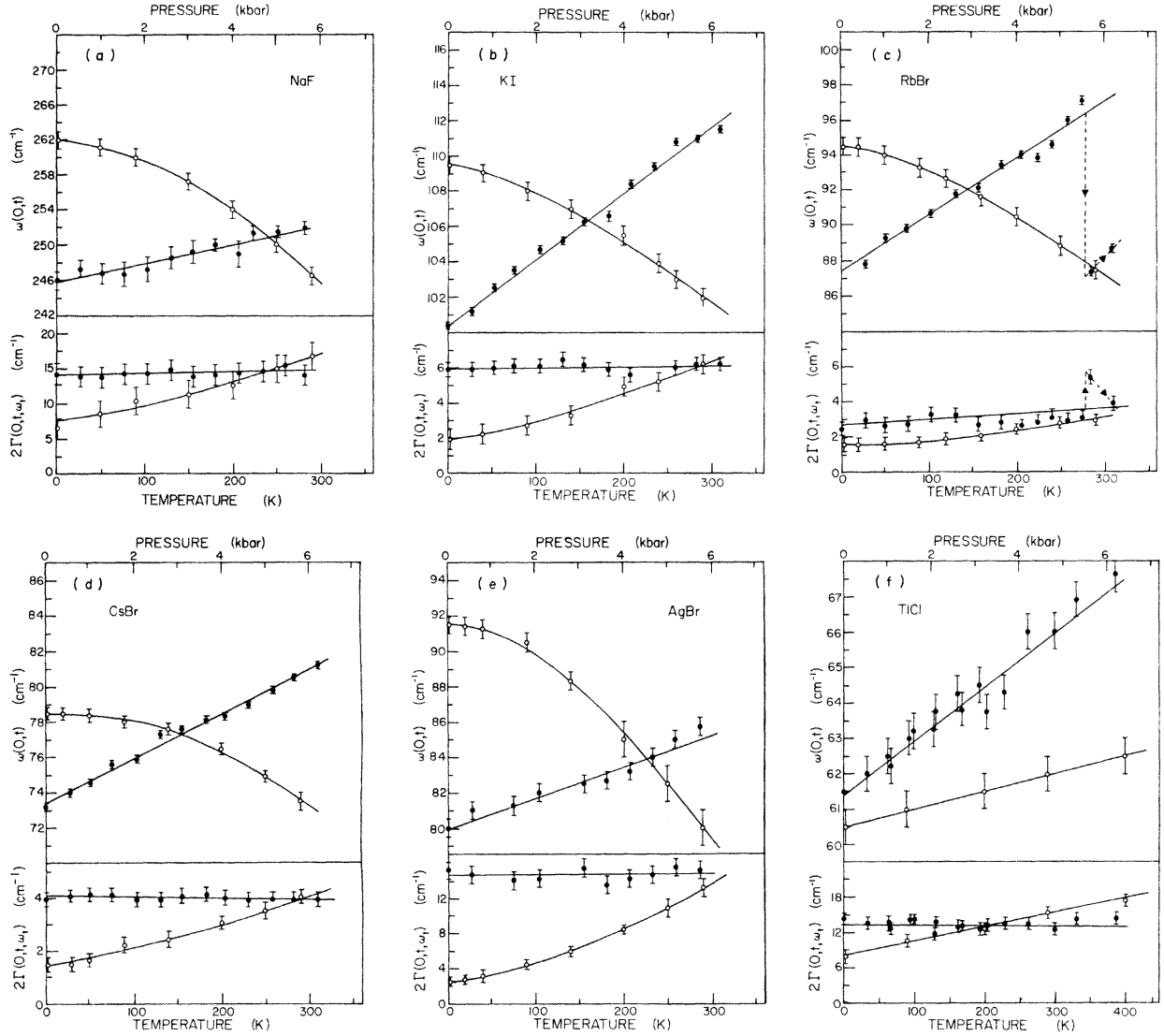

FIG. 6. Measured temperature (○) and pressure (●) dependence of $\omega(0, t)$ and $2\Gamma(0, t, \omega_t)$ for (a) NaF, (b) KI, (c) RbBr, (d) CsBr, (e) AgBr, and (f) TlCl. The broken line in (c) is for data taken in the high-pressure CsCl phase of RbBr.

which it has at 0 (K) and 1 bar pressure can be found from the thermal-strain expression

$$u^T = \int_0^T \alpha(T)\, dT = \tfrac{1}{3} \int_0^P \beta_T(P) dP\,, \qquad (46)$$

where $\alpha(T)$ and $\beta_T(P)$ are the linear thermal expansion and the isothermal compressibility of the crystal, respectively. Suitable values of $\alpha(T)$ and $\beta_T(P)$ were taken or deduced from the literature.[23-34, 39-46]

Using these estimates of $\omega_{T,P}(0, t)$ and the direct measurements of $\omega_{T,0}(0, t)$, we have determined $\Delta^E(0, t)$ and the function $A'(T)$ via Eqs. (36) and (41) and some of these results are shown for a few of the materials investigated in Fig. 7. With the exception perhaps of LiF, we do observe a linear temperature dependence of $A'(T)$ and we have used this to determine $\Delta_0^A(0, t, \omega_t')$, and hence $\Delta_T^A(0, t, \omega_t)$, as described in Sec. III A. Examples of the extrapolations used to determine $\Delta_0^A(0, t, \omega_t')$ and the consequent determination of the temperature dependence of $\Delta_T^A(0, t, \omega_t)$ are shown in Fig. 7.

A number of qualitative trends emerge from these results: (i) The $\Delta_0^A(0, t, \omega_t')$ are generally quite small, and are no more than a few percent of $\omega_{00}(0, t)$. (ii) The $\Delta_T^A(0, t, \omega_t)$ for the silver and alkali halides crystallizing in the NaCl structure are generally negative in sign at all temperatures and increase in magnitude with increasing temperature. (iii) The $\Delta_T^A(0, t, \omega_t)$ for the thallium and

TABLE VI. Measured temperature and pressure dependence of $\omega(0,t)$ for the alkali and heavy-metal halides. Also shown are the present experimental values of γ_t and previous values of γ_t.

	ω_t (cm^{-1})				$\frac{d\omega_t}{dP}$ ($cm^{-1}kbar^{-1}$)	γ_t	γ_t (Previous work)
T (K)	2	90	200	290	290	290	290
LiF	318.0±1.0	316.0±1.0	310.0±1.0	305.0±1.0	1.12±0.06	2.35±0.16	2.59 (Ref. 35)
LiCl	221.0±1.0	217.5±1.0	210.0±1.0	203.0±1.0			
LiBr	187.0±1.0	183.5±1.0	179.0±1.0	173.0±1.0			
LiI	151.5±1.0	150.0±1.0	146.0±1.0	142.0±1.0			
NaF	262.0±1.0	260.0±1.0	254.0±1.0	246.5±1.0	1.06±0.05	2.08±0.18	2.95 (Ref. 35)
NaCl	178.0±1.0	177.0±1.0	172.0±1.0	164.0±1.0	1.54±0.07	2.35±0.16	
NaBr	146.0±0.5	143.5±0.5	140.0±0.5	134.0±0.5	1.49±0.09	2.37±0.20	
NaI	123.0±1.0	121.5±0.8	118.5±0.8	115.2±0.5			
KF	201.5±1.0	200.5±1.0	197.5±1.0	194.0±1.0			
KCl	151.0±0.8	150.0±0.8	146.0±0.8	142.0±0.8	1.80±0.10	2.28±0.18	2.83±0.1 (Ref. 36)
KBr	123.0±0.5	122.0±0.5	118.0±0.5	114.0±0.5	1.59±0.07	2.06±0.13	2.46±0.1 (Ref. 36)
KI	109.5±0.5	108.0±0.5	105.5±0.5	102.0±0.5	1.88±0.01	2.20±0.06	3.1 (Ref. 37)
RbF	163.0±1.0	162.0±1.0	160.0±1.0	158.0±1.0			
RbCl	126.0±0.5	125.0±0.5	121.0±0.5	116.5±0.5	1.63±0.04	2.16±0.10	
RbBr	94.5±0.5	93.3±0.5	90.5±0.5	87.5±0.5	1.63±0.07	2.39±0.16	
RbI	81.6±0.5	80.4±0.5	77.0±0.5	75.5±0.5	1.48±0.08	2.09±0.15	2.5 (Ref. 37)
CsF	134.0±0.5	132.0±0.5	130.0±0.5	127.0±0.5			
CsCl	106.5±0.5	105.0±0.5	102.0±0.5	99.5±0.5	1.70±0.04	3.14±0.10	2.34±0.55 (Ref. 38)
CsBr	78.5±0.3	78.0±0.3	76.5±0.3	73.5±0.5	1.26±0.01	2.74±0.05	2.15±0.52 (Ref. 38)
CsI	65.8±0.3	65.5±0.3	64.0±0.3	62.1±0.3	1.20±0.03	2.42±0.08	1.90±0.58 (Ref. 38)
AgCl	121.0±1.0	117.5±1.0	112.5±2.0	105.0±2.0	1.07±0.03	4.34±0.16	5.0 ±1.0 (Ref. 9)
AgBr	91.5±0.5	90.5±0.5	85.0±1.0	80.0±1.0	0.89±0.03	4.41±0.19	5.6 ±1.1 (Ref. 9)
TlCl	60.5±0.5	61.0±0.5	61.5±0.5	62.0±0.5	0.96±0.04	3.62±0.20	3.9 ±0.8 (Ref. 9)
TlBr	45.0±0.3	45.5±0.3	46.4±0.5	47.0±0.5	0.90±0.02	4.30±0.16	3.8 ±0.8 (Ref. 9)

alkali halides crystallizing in the CsCl structure may be negative or positive at lower temperatures but are always positive at higher temperatures. (iv) The $\Delta_T^A(0,t,\omega_t)$ have a smaller temperature dependence than $\Delta^E(0,t)$ for all the materials studied except the thallium halides.

IV. DISCUSSION

Tables VIII–XIII summarize the experimental values reported here of $\Delta^E(0,t)$, $\Delta_T^A(0,t,\omega_t)$, and $\Gamma(0,t,\omega_t)$, as well as values of $\Delta^E(0,t)$ and $\Delta_T^A(0,t,0)$ derived from dielectric constant measurements reported earlier,[7] and compares these with the corresponding results from the theoretical calculations taken from Sec. II. Note that in this discussion we shall be comparing values of $\Gamma(0,t,\omega_t)$ and not the full spectral damping, $2\Gamma(0,t,\omega_t)$, reported in Sec. III. Before proceeding with a discussion of the comparison of these experimental and theoretical results, it is appropriate to attempt to assess the accuracies of the two kinds of results.

Given the approximations contained within the anharmonic theory, the errors associated with the calculated values of the anharmonic self-energies stem primarily from those involved with the $\omega^h(\vec{q},j)$ and the anharmonic force constants. The errors associated with the $\omega^h(\vec{q},j)$ are difficult to assess, but it can be stated that our lattice-dynamical calculations are in close agreement with available low-temperature dispersion curves, reported from inelastic neutron scattering experiments, with the most extreme differences being less than 10% over small regions of the Brillouin zone, and that anharmonic calculations for a few compounds using $\omega^h(\vec{q},j)$ values differing uniformly by 10% throughout the Brillouin zone lead to only 10% changes in the real and imaginary anharmonic self-energies. The anharmonic force constants are sensitive to the input values of r_0 and β, and in both cases values of these at low temperatures are needed. Values of β are typically determined directly at 4 K with an error of about ±2%. Such an error in β will lead to a 2% error in the A coefficient, a 2% error in the B coefficient and 1% error in the C coefficients listed in Table I. Although r_0 is usually determined quite precisely at 290 K to better than ±0.1% via x-ray measure-

TABLE VII. Measured temperature and pressure dependence of $2\Gamma(0,t,\omega_t)$ for the alkali and heavy-metal halides.

	$2\Gamma(0,t,\omega_t)$ (cm^{-1})				$\frac{d2\Gamma(0,t\ \omega_t)}{dP}$ ($cm^{-1}kbar^{-1}$)
T (K)	2	90	200	290	290
LiF	7.3±3.2	10.4±2.9	13.9±2.3	17.1±1.9	
LiCl	14.4±1.4	17.4±1.4	23.1±1.4	34.5±1.4	
LiBr	15.3±3.8	20.5±4.7	26.8±4.6	34.6±5.4	
LiI	25.0±4.7	27.9±4.7	35.0±7.5	39.7±8.8	
NaF	6.5±1.3	10.4±2.1	12.7±2.1	16.8±2.0	0.10±0.07
NaCl	2.5±0.7	3.5±0.7	5.3±0.5	7.0±0.5	−0.50±0.13
NaBr	3.4±0.9	4.3±0.7	7.0±0.7	8.4±0.7	−0.92±0.14
NaI	4.3±1.9	6.1±1.9	9.5±3.0	13.7±2.9	
KF	11.9±2.1	14.0±2.1	16.6±2.1	19.0±2.4	
KCl	1.4±0.6	1.9±0.4	3.4±0.5	4.5±0.4	−0.08±0.07
KBr	0.9±0.5	1.6±0.4	2.8±0.2	4.7±0.2	−0.03± 0.03
KI	2.0±0.6	2.7±0.5	5.0±0.5	6.2±0.5	0.03±0.02
RbF	6.4±0.9	7.4±1.2	9.6±1.3	10.9±1.3	
RbCl	2.5±0.4	3.1±0.4	4.0±0.4	4.8±0.4	−0.04±0.03
RbBr	1.3±0.3	1.7±0.3	2.4±0.3	3.0±0.3	0.14±0.11
RbI	1.1±0.2	1.4±0.2	2.1±0.2	2.8±0.2	0.12±0.04
CsF	9.2±1.4	9.9±2.0	16.2±2.0	19.7±2.0	
CsCl	3.4±0.5	3.7±0.5	5.1±0.5	6.1±0.5	−0.02±0.02
CsBr	1.5±0.2	2.3±0.2	3.1±0.2	4.0±0.2	−0.04±0.02
CsI	1.0±0.2	1.4±0.3	2.1±0.3	2.6±0.3	−0.04±0.02
AgCl	3.5±0.5	6.0±0.5	9.5±0.5	13.2±1.0	0.02±0.01
AgBr	2.5±0.5	4.5±0.5	8.5±0.5	13.2±1.0	0.04±0.02
TlCl	4.0±0.5	5.0±0.5	6.3±0.5	7.7±0.5	−0.05±0.04
TlBr	2.7±0.3	3.0±0.3	3.5±0.4	4.0±0.4	−0.03±0.02

ments, values of r_0 at lower temperatures are often not directly measured but are determined from the known 290-K value of r_0 and the known thermal-expansion data. This leads to a typical error of about ± 0.2% in r_0 at 4 K. Such an error will generate errors of the order of 10% for the A coefficient, 6% for the B coefficient, and 7% for the C coefficient. The accumulated errors in these coefficients will, of course, lead to errors in the individual contributions to the different total self-energy quantities. It should be recalled that $\Delta_T^A(0,t,\Omega)$ is obtained as a sum of $\Delta^{(4)}(0,t)$, $\Delta^{(8)}(0,t)$, $\Delta^{(6)}(0,t,\Omega)$, and $\Delta^{(8)}(0,t,\Omega)$, and although the errors on the individual contributions to the self-energy stemming from errors in r_0 and β are no larger than about 10%, the accumulated error on $\Delta_T^A(0,t,\Omega)$ is considerably larger because of the opposite signs of these individual contributions and because of the often close equivalence of the two dominant, but competing, terms $\Delta^{(4)}(0,t)$ and $\Delta^{(6)}(0,t,\Omega)$. However, $\Gamma(0,t,\Omega)$ is simply the sum of two components, $\Gamma^{(6)}(0,t,\Omega)$ and $\Gamma^{(8)}(0,t,\Omega)$, both of which are accurate to about ± 6%, and hence the accumulated error on $\Gamma(0,t,\Omega)$ will be smaller than that for $\Delta_T^A(0,t,\Omega)$. In Tables VIII–XIII we have listed our estimates of the possible errors associated with the different calculated self-energy components based on the known errors on r_0 and β only.

The errors on the experimental determinations of $\Delta^E(0,t)$, $\Delta_T^A(0,t,\Omega)$, and $\Gamma(0,t,\omega_t)$ can vary significantly. The errors on the measured $\omega_{T,0}(0,t)$ are generally quite small and at worst no larger than about ± 1%, but the errors on $\omega_{T,P}(0,t)$ will be somewhat larger than this due to the error in calculating P [see Eq. (46)]. The experimental and theoretical results strongly suggest that the zero-temperature anharmonic self-energies are quite small, so that the use of the approximation $\omega_{00}(0,t)\approx\omega^h(0,t)$ in Eqs. (36) and (41) should not generate errors of more than a few percent in the determinations. Consequently we believe that the determinations of $\Delta^E(0,t)$ and $A'(T)$ are generally accurate to better than ± 1.5 cm^{-1}. Of course, the determinations of $\Delta_T^A(0,t,\omega_t)$ are somewhat worse than this depending on the accuracy of the extrapolation procedure used to determine $\Delta_0^A(0,t,\omega_t')$. The errors on the measured $\Gamma(0,t,\omega_t)$ are determined to be no better than ± 15% for the longer phonon lifetimes and no

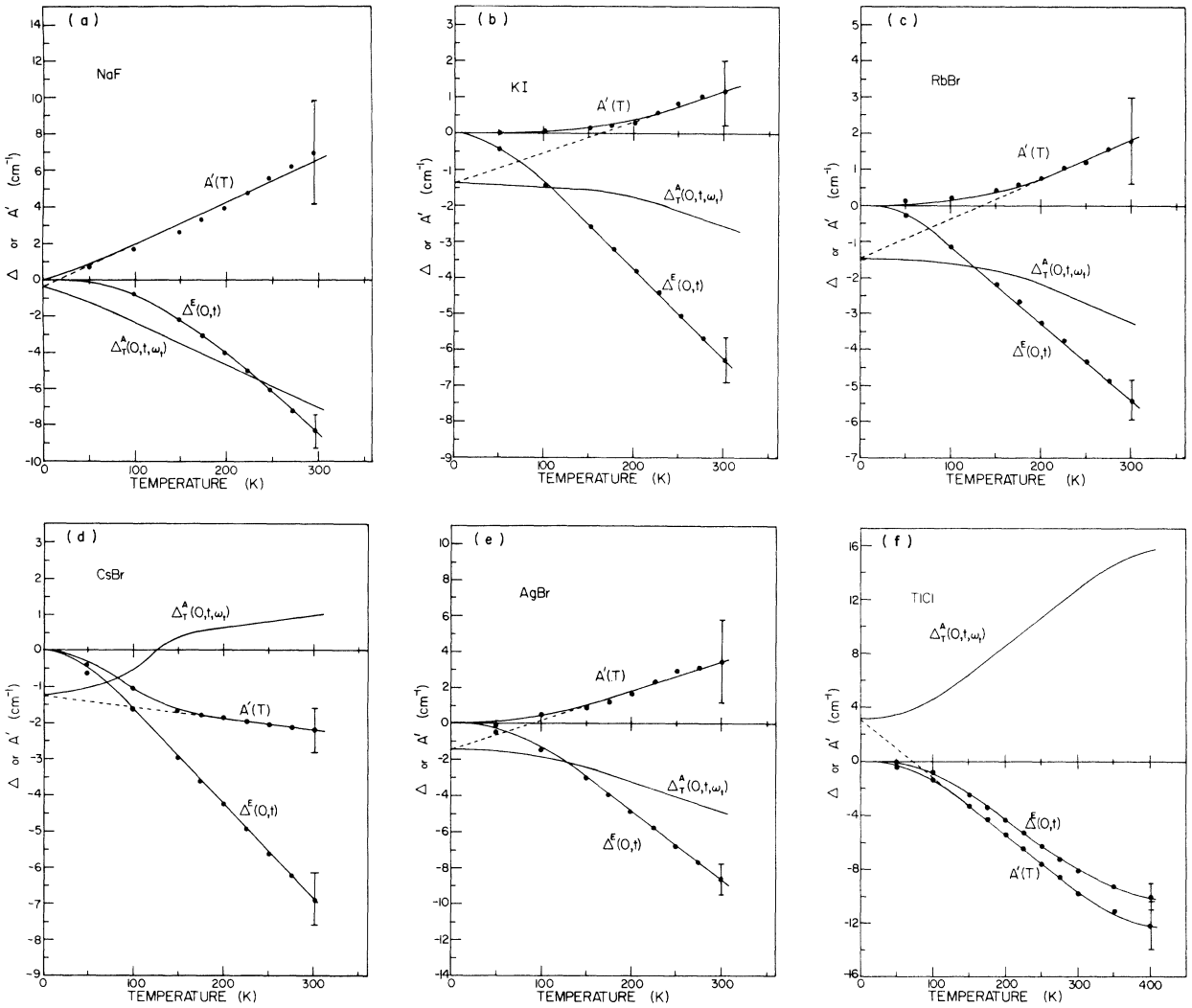

FIG. 7. Temperature dependence of $\Delta^E(0,t)$ and $\Delta_T^A(0,t,\omega_t)$ for (a) NaF, (b) KI, (c) RbBr, (d) CsBr, (e) AgBr, and (f) TlCl. The broken line shows the extrapolation of $A'(T)$ used to determine $\Delta_0^A(0,t,\omega_t')$.

better than ±25% for the shorter phonon lifetimes.

Bearing in mind the preceding comments on the accuracy of the different estimates of the anharmonic self-energy quantities, we turn now to a comparison of the experimental and theoretical results in Tables VIII–XIII. The experimental results have allowed separate determinations of $\Delta^E(0,t)$ to be made at $\Omega=0$ and $\Omega=\omega_t$. Equation (7) shows $\Delta^E(0,t)$ to be a frequency-independent quantity and the experimental results generally support this within the limits of the experimental accuracy. The exceptions to this are the results for the cesium and thallium halides at higher temperatures, but these differences may indicate the importance of the volume dependence of the dipole moments associated with the transverse-optic modes in these materials which have been neglected in the determination of $\Delta^E(0,t)$ at $\Omega=0$. It is for this reason that the results for $\Delta^E(0,t)$ determined at $\Omega=\omega_t$ are considered more reliable, and a comparison of these with the theoretical results reveals a good agreement within the accuracy limits for all the materials.

The results for $\Delta_T^A(0,t,0)$ are qualitatively very good in that both experiment and theory show a reversal in sign as the temperature is raised, and furthermore show this reversal to take place at about the same temperature. Quantitatively, the low-temperature results are in good agreement for all the materials and this reasonable agreement is maintained for the potassium and rubidium halides at higher temperatures. For the lithium and sodium halides, however, serious discrepancies arise between the two sets of data

TABLE VIII. Comparison of the calculated and experimental values, in cm^{-1}, of $\Delta^E(0,t)$, $\Delta_T^A(0,t,\Omega)$, determined at $\Omega=0$ and $\Omega=\omega_t$, and of $\Gamma(0,t,\omega_t)$ for the lithium halides.

		$\Delta^E(0,t)$			$\Delta_T^A(0,t,0)$		$\Delta_T^A(0,t,\omega_t)$			$\Gamma(0,t,\omega_t)$		
			Expt.				Calc.		Expt.	Calc.		Expt.
Ω	T (K)	Calc.	$\Omega=0$	$\Omega=(\omega_t)_{expt}$	Calc.	Expt.	$(\omega_t)_{calc}$	$(\omega_t)_{expt}$	$(\omega_t)_{expt}$	$(\omega_t)_{calc}$	$(\omega_t)_{expt}$	$(\omega_t)_{expt}$
LiF	5	0	0	0	2.0	0.8	− 1.1	− 1.1	0.2	0.3	0.4	3.7
	100	− 0.6	−0.5	− 0.4	0.8	−1.5	− 1.3	− 1.2	−1.5	0.8	0.8	5.4
	200	− 4.6	−2.7	− 3.7	− 5.1	−3.0	− 2.8	− 2.8	−3.0	3.7	3.8	7.0
	300	−10.9± 1.6	−8.2± 0.9	−11.4± 1.6	−11.8± 2.2	−4.5± 3.0	− 5.7± 3.7	− 5.5± 3.7	−4.4± 3.6	8.4± 0.5	8.8± 0.5	8.7± 1.5
LiCl	5	0	0		3.7	3.0	− 0.8	− 0.8		0.8	0.8	7.2
	100	− 4.1	−2.3		− 1.1	0.2	− 2.2	− 2.2		3.2	3.2	8.8
	200	−20.2	−5.8		−14.4	0.1	− 7.3	− 8.4		10.5	12.4	11.6
	300	−40.8± 6.1	−9.3± 1.4		−32.5± 4.2	0 ± 1.5	−17.1± 7.0	−19.8± 7.1		19.6± 1.2	23.2± 1.4	17.9± 3.0
LiBr	5	0			5.8		4.9	3.7		4.1	3.9	7.7
	100	− 6.7			− 0.3		− 0.4	0.5		10.1	10.7	10.6
	200	−26.7			−17.0		− 9.7	−14.6		12.2	28.3	13.4
	300	−50.5± 7.5			−43.6± 5.2		−40.7± 10.6	−40.3± 10.0		7.3± 0.4	43.6± 2.6	17.8± 3.7
LiI	5	0			6.4		− 8.4	5.1		0.1	0.2	12.5
	100	−12.8			− 7.9		−19.3	− 1.6		15.1	12.4	14.3
	200	−43.4± 6.4			−47.2± 5.5			−31.6± 9.3			47.0± 2.6	17.5± 3.8

TABLE IX. Comparison of the calculated and experimental values, in cm^{-1}, of $\Delta^E(0,t)$, $\Delta_T^A(0,t,\Omega)$, determined at $\Omega=0$ and $\Omega=\omega_t$, and of $\Gamma(0,t,\omega_t)$ for the sodium halides.

		$\Delta^E(0,t)$			$\Delta_T^A(0,t,0)$		$\Delta_T^A(0,t,\omega_t)$			$\Gamma(0,t,\omega_t)$		
			Expt.				Calc.		Expt.	Calc.		Expt.
	T (K)	Calc.	$\Omega=0$	$\Omega=(\omega_t)_{expt}$	Calc.	Expt.	$(\omega_t)_{calc}$	$(\omega_t)_{expt}$	$(\omega_t)_{expt}$	$(\omega_t)_{calc}$	$(\omega_t)_{expt}$	$(\omega_t)_{expt}$
NaF	5	0	0	0	1.6	2.2	−1.6	−1.9	−1.2	0.2	0.2	3.3
	100	− 0.6	−1.0	−0.7	0.2	0.2	−0.6	−0.8	−2.8	0.7	0.7	5.2
	200	− 3.7	−3.9	−4.4	− 3.9	−1.6	−1.1	−1.5	−5.2	2.2	2.3	6.4
	300	− 7.8 ± 1.2	−8.8 ± 1.3	−8.7 ± 1.0	− 8.2 ± 1.5	−2.5 ± 1.8	−2.3 ± 2.4	−2.3 ± 2.4	−7.7 ± 2.8	4.6 ± 0.3	4.7 ± 0.3	8.4 ± 1.0
NaCl	5	0	0	0	0.9	2.3	−0.7	−0.9	−1.4	0.3	0.3	1.3
	100	− 1.1	−1.3	−1.3	− 0.6	−0.2	−0.1	−0.5	−1.9	1.1	1.1	1.8
	200	− 4.6	−4.0	−3.3	− 4.6	−1.0	−0.6	−1.0	−3.3	2.8	3.2	2.7
	300	− 8.6 ± 1.3	−6.8 ± 1.0	−9.0 ± 0.5	− 9.0 ± 1.5	−1.5 ± 1.1	−1.6 ± 2.2	−1.8 ± 2.2	−5.0 ± 2.9	5.7 ± 0.4	5.7 ± 0.4	3.5 ± 0.3
NaBr	5	0	0	0	1.4	1.0	−0.3	−0.1	−3.2	0.7	1.3	1.7
	100	− 1.4	−1.5	−1.6	− 0.3	−0.6	−0.2	−0.8	−3.6	2.1	2.7	2.2
	200	− 5.0	−1.9	−4.7	− 3.3	−1.2	0.4	−1.4	−4.5	4.8	5.4	3.5
	300	− 9.0 ± 1.3	−6.0 ± 0.8	−7.9 ± 0.5	− 7.7 ± 1.5	−1.8 ± 1.4	0.1 ± 2.2	−1.3 ± 2.3	−6.5 ± 1.6	8.4 ± 0.5	8.5 ± 0.5	4.2 ± 0.4
NaI	5	0	0		1.9	1.1	1.7	1.7		0.7	0.7	2.2
	100	− 1.8	−1.7		0	−0.3	3.0	3.0		3.8	3.7	3.1
	200	− 5.9	−4.6		− 4.2	−0.7	2.1	1.4		10.0	9.6	4.8
	300	−10.4 ± 1.5	−6.8 ± 1.0		−11.3 ± 1.9	−1.0 ± 0.5	−3.6 ± 2.9	1.2 ± 2.8		14.9 ± 0.9	16.9 ± 1.0	6.9 ± 1.5

TABLE X. Comparison of the calculated and experimental values, in cm^{-1}, of $\Delta^E(0,t)$, $\Delta_T^A(0,t,\Omega)$, determined at $\Omega=0$ and $\Omega=\omega_t$, and of $\Gamma(0,t,\omega_t)$ for the potassium halides.

		$\Delta^E(0,t)$			$\Delta_T^A(0,t,0)$		$\Delta_T^A(0,t,\omega_t)$			$\Gamma(0,t,\omega_t)$		
			Expt.				Calc.		Expt.	Calc.		Expt.
	T (K)	Calc.	$\Omega=0$	$\Omega=(\omega_t)_{expt}$	Calc.	Expt.	$(\omega_t)_{calc}$	$(\omega_t)_{expt}$	$(\omega_t)_{expt}$	$(\omega_t)_{calc}$	$(\omega_t)_{expt}$	$(\omega_t)_{expt}$
KF	5	0			2.1		−0.1	−0.1		0.5	0.5	5.9
	100	−1.1			−0.1		−0.3	−0.3		1.3	1.3	7.0
	200	−5.2			−4.4		−0.9	−0.9		3.6	3.6	8.3
	300	−10.2 ± 1.5			−9.6 ± 1.7		−2.1 ± 2.7	−2.1 ± 2.8		7.0 ± 0.4	6.9 ± 0.4	9.5 ± 1.2
KCl	5	0	0	0	1.21	0.2	−0.1	−0.1	−1.1	0.2	0.2	0.7
	100	−1.1	−1.0	−1.2	−0.56	−2.2	−0.1	−0.1	−1.1	0.8	0.8	1.0
	200	−4.0	−3.5	−4.3	−3.33	−4.5	−0.6	−0.6	−1.6	2.6	2.6	1.7
	300	−7.4 ± 1.1	−6.3 ± 0.9	−7.6 ± 1.2	−6.82 ± 2.0	−6.9 ± 2.7	−1.4 ± 2.0	−1.4 ± 2.0	−2.4 ± 2.4	4.8 ± 0.3	4.8 ± 0.3	2.3 ± 0.2
KBr	5	0	0	0	1.1	0.7	0.5	0.5	−2.0	0.6	0.6	0.5
	100	−1.1	−1.0	−0.9	−0.2	−1.6	1.0	0.8	−2.3	2.0	2.0	0.9
	200	−3.8	−3.2	−3.3	−2.2	−3.3	0.7	0.7	−3.6	4.2	4.1	1.4
	300	−6.7 ± 1.0	−5.4 ± 0.6	−5.8 ± 0.6	−5.0 ± 1.1	−4.8 ± 2.0	−0.3 ± 1.7	0 ± 1.7	−5.5 ± 1.6	6.6 ± 0.4	5.7 ± 0.3	2.4 ± 0.1
KI	5	0	0	0	0.8	1.2	0.7	0.7	−1.4	0.2	0.2	1.0
	100	−0.9	−0.9	−1.3	0.2	−1.4	1.6	1.7	−1.5	0.9	0.9	1.5
	200	−2.9	−2.9	−3.7	−0.7	−3.0	2.6	3.0	−1.7	2.4	2.4	2.6
	300	−5.0 ± 0.7	−5.0 ± 0.5	−6.2 ± 0.6	−2.2 ± 0.7	−4.5 ± 1.2	3.1 ± 0.9	3.9 ± 0.9	−2.5 ± 1.6	4.0 ± 0.3	4.8 ± 0.3	3.1 ± 0.3

TABLE XI. Comparison of the calculated and experimental values, in cm^{-1}, of $\Delta^E(0,t)$, $\Delta_T^A(0,t,\Omega)$, determined at $\Omega=0$ and $\Omega=\omega_t$, and of $\Gamma(0,t,\omega_t)$ for the rubidium halides.

		$\Delta^E(0,t)$			$\Delta_T^A(0,t,0)$		$\Delta_T^A(0,t,\omega_t)$			$\Gamma(0,t,\omega_t)$		
			Expt.				Calc.		Expt.	Calc.		Expt.
	T (K)	Calc.	$\Omega=0$	$\Omega=(\omega_t)_{expt}$	Calc.	Expt.	$(\omega_t)_{calc}$	$(\omega_t)_{expt}$	$(\omega_t)_{expt}$	$(\omega_t)_{calc}$	$(\omega_t)_{expt}$	$(\omega_t)_{expt}$
RbF	5	0			2.9		1.3	1.4		0.9	0.9	3.2
	100	−2.0			0.7		1.0	1.0		3.2	3.2	3.8
	200	−7.5			−3.7		−0.8	−1.5		7.1	7.9	4.8
	300	−13.8 ± 2.1			−10.2 ± 2.1		−2.6 ± 3.4	−6.1 ± 3.8		11.6 ± 0.7	13.1 ± 0.7	5.5 ± 0.7
RbCl	5	0	0	0	1.5	0.6	0.2	0.2	−3.5	0.6	0.6	1.3
	100	−1.6	−0.9	−1.1	−0.1	−1.4	0	−0.1	−3.7	1.7	1.9	1.6
	200	−5.2	−2.8	−3.4	−2.9	−2.7	−0.3	−0.5	−5.1	3.8	3.9	2.0
	300	−9.2 ± 1.8	−4.5 ± 0.5	−5.9 ± 0.6	−7.0 ± 1.6	−4.2 ± 1.5	−1.6 ± 2.6	−1.6 ± 2.6	−7.6 ± 1.6	6.5 ± 0.4	6.7 ± 0.4	2.6 ± 0.2
RbBr	5	0	0	0	0.7	−0.1	0.1	0.1	−1.4	0.2	0.2	0.7
	100	−1.3	−1.1	−1.1	−0.7	−1.2	0	0	−1.7	1.3	1.3	0.9
	200	−3.9	−3.0	−3.2	−2.7	−1.8	−0.5	−0.7	−2.2	2.2	2.3	1.2
	300	−6.5 ± 1.0	−4.8 ± 0.5	−5.4 ± 0.5	−5.6 ± 1.0	−2.6 ± 1.1	−1.1 ± 1.5	−1.1 ± 1.5	−3.2 ± 1.5	4.4 ± 0.3	4.4 ± 0.3	1.5 ± 0.2
RbI	5	0	0	0	0.6	−0.7	1.9	1.9	−0.5	0.3	0.3	0.6
	100	−1.3	−0.9	−1.0	−0.5	−1.9	0.4	0.3	−0.9	1.4	1.4	0.8
	200	−3.5	−2.4	−2.8	−2.2	−2.8	0.2	0.5	−1.7	2.5	2.6	1.1
	300	−5.9 ± 0.9	−3.7 ± 0.4	−4.5 ± 0.4	−4.6 ± 0.9	−4.1 ± 1.5	−0.2 ± 1.4	−0.2 ± 1.4	−2.5 ± 1.4	4.6 ± 0.3	4.7 ± 0.3	1.5 ± 0.1

TABLE XII. Experimental values, in cm^{-1}, of $\Delta^E(0,t)$ and $\Delta_T^A(0,t,\Omega)$, determined at $\Omega=0$ and $\Omega=\omega_t$, for the cesium halides.

		$\Delta^E(0,t)$			
	T (K)	$\Omega=0$	$\Omega=\omega_t$	$\Delta_T^A(0,t,0)$	$\Delta_T^A(0,t,\omega_t)$
CsCl	5	0	0	−1.1	−0.7
	100	−1.6	−2.0	1.2	−0.1
	200	−2.9	−5.8	3.5	1.5
	300	−3.8 ± 0.4	−9.8 ± 1.0	5.1 ± 2.4	2.3 ± 2.0
CsBr	5	0	0	0.4	−1.2
	100	−1.2	−1.6	0.8	−0.2
	200	−3.2	−4.2	1.7	0.6
	300	−5.2 ± 0.6	−6.8 ± 0.7	2.6 ± 1.5	0.9 ± 1.5
CsI	5	0	0	0.2	0.5
	100	−1.0	−1.4	0.5	1.3
	200	−2.3	−3.4	1.0	1.8
	300	−3.7 ± 0.4	−5.5 ± 0.5	1.4 ± 1.3	2.2 ± 1.1

at higher temperatures, with the calculated results showing a much stronger temperature dependence.

The agreement between theory and experiment is less good for $\Delta_T^A(0,t,\omega_t)$. Qualitatively, the experimental results suggest that the second-order anharmonic contributions always dominate so that $\Delta_T^A(0,t,\omega_t)<0$, whereas the calculated results reveal that this is not always so at the lower temperatures. Quantitatively, although the results for many of the compounds agree within the error limitations, the experimental results generally tend to vary somewhat faster with temperature than the calculated theoretical predictions. The preceding comments have been made for the calculated values of $\Delta_T^A(0,t,\omega_t)$ determined at the calculated value of ω_t. In order to test the sensitivity of the calculated values of $\Delta_T^A(0,t,\omega_t)$ to any frequency dispersion, we have also listed values of $\Delta_T^A(0,t,\omega_t)$ calculated at the experimentally determined values of ω_t in Tables VIII–XI. With the exception of the higher temperature data for LiBr and LiI (which in any case must be treated with some caution for the reasons given earlier), the two sets of calculated values for $\Delta_T^A(0,t,\omega_t)$ are quite close and generally differ at most by no more than ±15%. However, the values of $\Delta_T^A(0,t,\omega_t)$ calculated at $(\omega_t)_{\text{exp}}$ are generally in no better agreement with the experimental values than the $\Delta_T^A(0,t,\omega_t)$ calculated at $(\omega_t)_{\text{calc}}$.

The results for $\Gamma(0,t,\omega_t)$ show the theoretical predictions at low temperatures to usually be

TABLE XIII. Experimental values, in cm^{-1}, of $\Delta^E(0,t)$ and $\Delta_T^A(0,t,\Omega)$, determined at $\Omega=0$ and $\Omega=\omega_t$, for the silver and thallium halides.

		$\Delta^E(0,t)$			
	T (K)	$\Omega=0$	$\Omega=\omega_t$	$\Delta_T^A(0,t,0)$	$\Delta_T^A(0,t,\omega_t)$
AgCl	5	0	0	3.5	− 4.5
	100	− 0.8	−1.7	0.3	− 5.3
	200	− 3.7	−5.2	−2.1	− 7.2
	300	− 8.8 ± 0.8	−9.5 ± 1.0	−3.0 ± 2.0	−10.5 ± 5.0
AgBr	5	0	0	3.0	− 1.4
	100	− 0.6	−1.3	−0.3	− 2.0
	200	− 5.2	−4.6	−0.7	− 3.2
	300	−11.2 ± 0.8	−8.6 ± 0.8	−1.2 ± 2.0	− 4.8 ± 2.3
TlCl	5	0	0	1.0	3.0
	100	− 0.6	−0.9	3.9	4.5
	200	− 3.4	−4.4	7.1	8.4
	300	− 4.6 ± 0.7	−8.3 ± 1.0	10.8 ± 2.0	12.6 ± 2.1
TlBr	5	0	0	1.0	3.0
	100	− 0.6	−0.6	3.1	4.4
	200	− 2.0	−3.5	6.0	8.6
	300	− 4.3 ± 0.6	−7.6 ± 0.9	8.8 ± 2.0	12.8 ± 1.8

somewhat smaller than the experimental values and, as the temperature is increased, to generally have a somewhat faster temperature dependence than the experimental results. The calculated theoretical results at the higher temperatures are generally in reasonable agreement with the experimental results for the lithium and sodium halides but are significantly bigger than the experimental results for the potassium and rubidium halides.

The experimental studies of the pressure dependence of $\Gamma(0, t, \omega_t)$ suggest that its volume dependence is small. Equations (17) and (18) reveal that such a volume dependence can arise only from that of the anharmonic coupling coefficients or from that of the $\omega^h(\vec{q}, j)$. We have attempted to calculate approximately what Eqs. (17) and (18) would predict for the volume dependence of $\Gamma(0, t, \omega_t)$ for a number of alkali halides by allowing all the $\omega^h(\vec{q}, j)$ to have the same pressure dependence as that measured for $\omega(0, t)$ and by using values of γ_0 and β suitably corrected for the effects of pressure. Such assumptions lead to the conclusion that $\Gamma(0, t, \omega_t)$ will always decrease with increasing pressure by (1–2)% per kbar. Although the absolute magnitude of this calculated pressure dependence for $\Gamma(0, t, \omega_t)$ is in agreement with that found experimentally, these results do not explain the small increases with pressure found for $\Gamma(0, t, \omega_t)$ for some materials.

The reason for the less good agreement between the calculated and experimental anharmonic self-energies at $\Omega = \omega_t$ is not clear. The discrepancy between calculation and experiment for $\Gamma(0, t, \omega_t)$ at low temperatures could simply arise from an underestimate of $\Gamma^{(6)}(0, t, \omega_t)$ or $\Gamma^{(8)}(0, t, \omega_t)$ or from some sample artifact in the low-temperature experimental measurements; this latter would seem most unlikely, however, in view of the equivalent results that we obtain from single-crystal reflection measurements and thin-film transmission measurements. The generally good agreement between calculation and experiment for the higher temperature $\Gamma(0, t, \omega_t)$ for the sodium, potassium, and rubidium halides suggests, but does not prove, that the calculated form of $\tilde{\Delta}^A(0, t, \omega_t)$ may be correct [see Eq. (18)]; if this were true then this in turn would suggest that the general disagreement between calculation and experiment for $\Delta_T^A(0, t, \omega_t)$ might arise from the calculation of $\Delta^A(0, t)$ [see Eq. (8)].

V. CONCLUSIONS

In this paper we have presented both experimental and calculated theoretical results for the self-energies associated with the $q \approx 0$ transverse-optic modes of a wide range of simple ionic solids. The comparison between experiment and theory is generally good for the thermal-strain contributions and for the low-frequency anharmonic self-energies. However, some discrepancies between experiment and theory occur for some materials for the far-infrared anharmonic self-energies which may not be due simply to the associated errors of the experiments or calculations. However, before reconsideration of the current calculation procedures and the anharmonic theories are undertaken, it would seem that experimental measurements of the full frequency dependence of the anharmonic self-energies should be attempted in order to more fully test the full frequency dependence of the anharmonic self-energy calculations. Given the experimental results presented in this paper for the thermal-strain contribution, it would now seem possible to utilize such techniques as asymmetric Fourier-transform spectroscopy[47] to yield the full dispersion of the dielectric response and hence derive the frequency dependence of the anharmonic self-energies following the procedure outlined by Lowndes and Martin.[7]

ACKNOWLEDGMENTS

We would like to thank Professor D. H. Martin for valuable discussions at the outset of this work. We would also like to thank S. Pai for completing some of the high-pressure experiments and J. Weisz for preparing and studying the influence of pressure on several of the materials investigated on this work. Finally, we thank J. Weston of Queen Mary College, University of London, for his very valuable help in fabricating the prototype high-pressure far-infrared cell, and J. Sanroma of this department for his expert assistance in fabricating the present cell.

---

*Research supported by a grant from the Army Research Office, Durham, N.C., and by a grant from the Research Corporation. Part of the equipment used in this work was provided under NASA Cooperative Agreement NCAw 22-011-079.

†Work initiated at Queen Mary College, University of London.

[1]A. A. Maradudin and A. E. Fein, Phys. Rev. 128, 2589 (1962).

[2]R. A. Cowley, Adv. Phys. 12, 421 (1963).

[3]I. P. Ipatova, A. A. Maradudin, and R. F. Wallis, Phys. Rev. 155, 882 (1967).
[4]K. W. Johnson and E. E. Bell, Phys. Rev. 187, 1044 (1969).
[5]E. R. Cowley, J. Phys. C 5, 1345 (1972).
[6]A. Rastogi, J. P. Hawranek, and R. P. Lowndes, Phys. Rev. B 9, 1938 (1974).
[7]R. P. Lowndes and D. H. Martin, Proc. R. Soc. Lond. A 316, 351 (1970).
[8]R. P. Lowndes, Phys. Rev. Lett. 27, 1134 (1971).
[9]R. P. Lowndes, Phys. Rev. B 6, 1490 (1972).
[10]G. Leibfried and W. Ludwig, Solid State Phys. 12, (1961).
[11]B. Szigeti, Proc. R. Soc. Lond. A 252, 217 (1959).
[12]B. Szigeti, Proc. R. Soc. Lond. A 258, 377 (1960).
[13]H. Bilz, in *Phonons in Perfect Lattices and in Lattices with Point Imperfections*, edited by R. W. H. Stevenson (Oliver and Boyd, Edinburgh, 1966), p. 208.
[14]R. F. Wallis, I. P. Ipatova, and A. A. Maradudin, Fiz. Tverd. Tela 8, 1064 (1966) [Sov. Phys.-Solid State 8, 850 (1966)].
[15]R. E. Peierls, *Quantum Theory of Solids* (Oxford U.P., Oxford, 1956), p. 38.
[16]U. Schröder, Solid State Commun. 4, 347 (1966).
[17]J. R. Hardy and A. M. Karo, in *Proceedings of the International Conference on Lattice Dynamics*, edited by R. F. Wallis (Pergamon, London, 1964), p. 195.
[18]M. Born and K. Huang, *Dynamical Theory of Crystal Lattices* (Oxford U.P., Oxford, 1954), p. 124.
[19]R. P. Lowndes and D. H. Martin, Proc. R. Soc. Lond. A 308, 473 (1969).
[20]C. E. Weir E. R. Lippincott, A. van Valkenburg, and E. N. Bunting, J. Res. Natl. Bur. Stand. (U.S.) A 63, 55 (1959).
[21]E. E. Havinga and A. J. Bosman, Phys. Rev. 140, A 292 (1965).
[22]G. O. Jones, D. H. Martin, P. A. Mawer, and C. H. Perry, Proc. R. Soc. Lond. A 261, 10 (1961).
[23]J. K. Galt, Phys. Rev. 73, 1460 (1948).
[24]C. V. Briscoe and C. F. Squire, Phys. Rev. 106, 1175 (1957).
[25]M. H. Norwood and C. V. Briscoe, Phys. Rev. 112, 45 (1958).
[26]B. J. Marshall, Phys. Rev. 121, 72 (1961).
[27]R. Fuchs, MIT Technical Report No. 167, 1961 (unpublished).
[28]J. Vallin, O. Beckman, and K. Salama, J. Appl. Phys. 35, 1222 (1964).
[29]J. T. Lewis, A. Lehoczky, and C. V. Briscoe, Phys. Rev. 161, 877 (1967).
[30]B. J. Marshall, D. O. Pederson, and G. A. Dorris, J. Phys. Chem. Solids 28, 1061 (1967).
[31]J. Vallin, K. Marklund, and J. O. Sikstrom, Ark. Fys. 33, 345 (1967).
[32]W. Hidshaw, J. T. Lewis, and C. V. Briscoe, Phys. Rev. 163, 876 (1967).
[33]K. F. Loje and D. E. Schuele, J. Phys. Chem. Solids 31, 2051 (1970).
[34]M. P. Tosi, Solid State Phys. 16, 44 (1964).
[35]S. S. Mitra, C. Postmus, and J. R. Ferraro, Phys. Rev. Lett. 18, 455 (1967).
[36]C. Postmus, J. R. Ferraro, and S. S. Mitra, Phys. Rev. 174, 983 (1968).
[37]J. R. Ferraro, S. S. Mitra, and A. Quattrochi, J. Appl. Phys. 42, 3677 (1971).
[38]R. P. Lowndes, in *Proceedings of the International Conference on Phonons at Rennes*, edited by M. A. Nusimovici (Flammarion, Paris, 1971), p. 473.
[39]F. A. Henglein, Z. Phys. Chem. A 115, 91 (1925).
[40]B. Yates and C. H. Panter Proc. Phys. Soc. Lond. 80, 373 (1962).
[41]B. R. Lawn, Acta Crystallogr. 16, 1163 (1963).
[42]G. K. White, Proc. R. Soc. Lond. A 286, 204 (1965).
[43]B. W. James and B. Yates, Philos. Mag. 12, 253 (1965).
[44]A. C. Bailey and B. Yates, Philos. Mag. 16, 1241 (1967).
[45]R. F. Cooper and B. Yates, J. Phys. C 4, L 113 (1971).
[46]A. D. Redmond and B. Yates, J. Phys. C 5, 1589 (1972).
[47]J. E. Chamberlain, J. E. Gibbs, and M. A. Gebbie, Nature 198, 874 (1963).

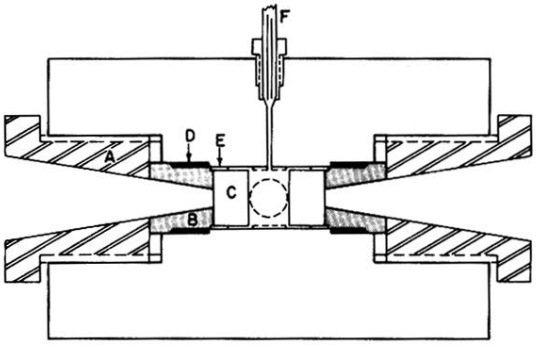

FIG. 3. High-pressure far-infrared cell. A, retaining closure; B, window mount; C, window; D, packing; E, window retaining ring; F, gas input line.